Road surface texture measurement using digital image processing and information theory

B. Pidwerbesky, J. Waters
Fulton Hogan Limited, Christchurch, New Zealand

D. Gransberg, R. Stemprok
University of Oklahoma, USA

Land Transport New Zealand Research Report 290

ISBN 0-478-28701-X
ISSN 1177-0600

PO Box 2840, Waterloo Quay, Wellington, New Zealand
Telephone 64-4 931 8700; Facsimile 64-4-931 8701
Email: *research@landtransport.govt.nz*
Website: *www.landtransport.govt.nz*

Pidwerbesky, B.[1], Waters, J.[1], Gransberg, D.[2], Stemprok, R.[2] 2006. Road surface texture measurement using digital image processing and information theory. *Land Transport New Zealand Research Report 290*. 65pp.

[1] Fulton Hogan Ltd, PO Box 39185, Harewood, Christchurch, New Zealand.
[2] University of Oklahoma, Norman, Oklahoma, USA.

Keywords: chipseal, digital image processing, macrotexture, information theory, road, road surface, sand circle test, surface texture, texture measurement

An important note for the reader

Land Transport New Zealand is a crown entity established under the Land Transport Management Act 2003. The objective of Land Transport New Zealand is to allocate resources and to undertake its functions in a way that contributes to an integrated, safe, responsive and sustainable land transport system. Each year, Land Transport New Zealand invests a portion of its funds on research that contributes to this objective.

The research detailed in this report was commissioned by Land Transport New Zealand.

While this report is believed to be correct at the time of its preparation, Land Transport New Zealand, and its employees and agents involved in its preparation and publication, cannot accept any liability for its contents or for any consequences arising from its use. People using the contents of the document, whether directly or indirectly, should apply and rely on their own skill and judgement. They should not rely on its contents in isolation from other sources of advice and information. If necessary, they should seek appropriate legal or other expert advice in relation to their own circumstances, and to the use of this report.

The material contained in this report is the output of research and should not be construed in any way as policy adopted by Land Transport New Zealand but may be used in the formulation of future policy.

Contents

Executive summary

Background

The New Zealand seal design algorithm requires texture depth of the existing surface as a key input. This texture has been measured using a volumetric technique called the sand circle test. Even with experienced, skilled operators, the test takes some time to perform, and is normally done in live traffic conditions with varying levels of traffic control. Even though the reproducibility (40%) of the sand circle test is poor, it is the most common means to measure texture.

The purpose of this research was to evaluate whether a practical method of road surface texture measurement using digital image processing, incorporating information theory and fast Fourier transform (FFT) analysis could be developed. The objectives of the research, which was carried out in Oklahoma, USA, and Christchurch, New Zealand in 2004 and 2005, were to develop:

- an accurate, repeatable method of measuring texture to replace the sand circle method,
- a fast, safe method of measuring texture to reduce the operator risk associated with road surface texture measurement and minimise disruption to traffic.

Similar research has been undertaken in Texas, USA, but the focus of the American research was to correlate a qualitative performance rating of the chipseal pavement with a quantitative measure of texture derived from digital information. This research aimed to extend the previous research by applying the imaging concept for measuring chipseal texture depth, in order to ultimately replace the present sand circle method of measuring texture in use in New Zealand.

The objective parameter selected to quantify the surface condition was the information content of each image as calculated by a FFT, discussed in detail in the report. In essence, each image has a finite amount of information contained in its boundaries. This information can be measured by determining the relative change in luminance intensity between adjoining pixels in the image. This relative difference in luminance is called the spatial frequency. High contrast occurs at the boundaries between two different objects in an image. Thus, in the chipseal image, the contrast is formed by the amount of light reflected off the exposed aggregate against the amount of light reflected off the background formed by the bitumen. It was obvious to the naked eye that the difference between chipseal performance success and failure had to do with the relationship between the aggregate and the surrounding bitumen. Therefore, it was postulated that the surface condition could be measured by correlating the information content of a digital image to the qualitative rating of the human expert in the previous Texas study and to a sand circle texture measurement in this particular study.

Research methodology

Standard commercial software was utilised to process the digital images of chipseal test sections. The processing of the chipseal images consisted of filtering the information content found in the images and quantifying this filtered information. This information intuitively seeks to differentiate surface texture on a basis of visual information content. As a result, the process contains a built-in check on image processing output: the ability to qualitatively confirm that images of like visual texture (i.e. satisfactory, flushed, etc.) are also yielding similar FFT numbers as well as similar sand circle measurements.

The research methodology consisted of the following steps:

- A standardised camera set-up was developed for use in the field measurements.
- Chipseal test sections were identified and a data collection plan was implemented.
- Digital images were taken in the field and sand circle measurements were then taken in the same location as the image. Laser devices were not used to measure texture because an average texture value from a volumetric test, which lasers cannot provide, was required.
- The images were processed and an FFT value was obtained for each 'ring' in the digital image (i.e. concentric rings of pixels surrounding a central pixel).
- The 'ring' FFT values were then statistically correlated with their corresponding sand circle measurements using linear regression techniques and the coefficient of determination (R^2 value) as the objective measure of correlation.
- Once each ring had been tested individually, groups of rings were tested to determine if the behaviour of the imaging was better described in sets rather than individually.
- Those rings and groups of rings that exhibited the strongest correlation were then explored in depth to identify the most promising measures of texture via imaging.

The output is a regression equation that describes the best fit of a curve that represents the relationship of the change in texture with respect to the change in FFT values.

Synopsis of findings and results

The research extended the previous correlation between digital image output and qualitative chipseal surface condition ratings, to a quantitative correlation between the digital image output and a physical texture measurement made by the sand circle test. A statistical correlation based on the coefficient of determination (R^2) of 0.93 for the data was obtained in the preliminary investigation. This was for digital image output measured by the sum of the FFT values in ring 3 of the images.

The images were then divided into a large number of rings based on spatial frequencies. The graphical representation of the processed imagery output visually indicated that the major variation between images of differing texture occurred in the first 25 rings. Thus, the research focused on this particular area of output and was able to obtain a statistical correlation based the coefficient of determination (R^2) of 0.80 for the average FFT value in

concentric rings 1 to 25, proving that field measurements of chipseal texture can generate a measurable mathematical relationship in a digital image.

The best correlation appeared to be with the average of the sum of FFT values in rings 1 to 25 versus the texture. The correlation was with essentially the entire variable portion of the digital image. Thus, it confirms the principle that the information content of a digital image can accurately portray the chipseal condition at that point on the road's surface.

The report details seven major and eight minor conclusions, the most important of which are:

1. The results clearly demonstrated that the merger of digital image processing and physical texture measurements is possible and the potential to successfully replace the sand circle test with a digital camera is high. The researchers were able to validate both the concept and the principle through the initial set of experiments. These allowed the team to standardise the experimental set-up and calibrate the software and hardware necessary to achieve strong correlation using linear regression analysis with a sorted sample population.

2. The major goal of the research was to prove that a relationship exists between chipseal texture (as measured by the sand circle test) and digital image output (as measured by a function of the FFT of the digital image). Therefore, the correlations were sought in both directions, i.e. texture versus FFT and FFT versus texture. Additionally, the texture component was looked at in two ways: using the sand circle diameter and the computed texture depth. Two strong correlations between image output and physical measurements were found:

    a. When the calculated texture depth was taken as the independent variable and a linear regression equation of the best fit curve was developed using the average of the sums of FFT values in rings 1 to 25, a coefficient of determination (R^2) of 0.80 was derived indicating that the texture depth explains approximately 80% of the variations observed in the FFT component to the regression analysis. The equation is a second order polynomial:

    $$y = 41146x^2 - 99229x + 353440$$

    This conclusively confirms the notion that physical texture can generate a measurable function in a digital image.

    b. Using higher order polynomials for the regression equation tends to increase the R^2 values for most situations. However, they generate complex curves that will be difficult to use in eventual field applications. A linear relationship would be preferred to simplify moving this technology from research to field application. The linear regression of the relationship described in subparagraph 2a above

yields an R^2 value of 0.52, not much better than the 0.40 reproducibility of the sand circle test.

3. The technology's ability to measure and correlate the difference between satisfactory texture and texture that is flushed is excellent. Thus, the chipseal failure condition corresponding to a pavement surface condition that is of greatest danger to the travelling public appears to be covered by the proposed technology.

Limitations of the research

The strong statistical correlations prove the hypothesis that a physical relationship exists between chipseal texture and the FFT values of a digital image. At present, however, the correlation is quite fragile because the requirement to remove data points from the population for chipseals that were not the same type and size as the grade 3 single seal reduced the available set of data points for analysis. Thus, the major issue that will need to be addressed in the future is the need to strengthen the correlation by significantly increasing the total size of the sample population.

.

Abstract

This report details the progress made in tests in Oklahoma, USA and Christchurch, New Zealand during the period August 2004 to June 2005, exploring digital imaging technology to measure chipseal surface texture. It details the research methodology to develop a technology to replace the sand circle test as a means to measure chipseal surface texture more accurately and safely. The project used digital imagery and exploited 'information theory' to develop a quantitative relationship between texture measured by the sand circle test and the fast Fourier transform of a digital image of the surface taken at the same spot as the test. The preliminary correlation achieved and reported in the interim report has been confirmed by a larger group of data collected after the interim report was written. A reliable statistical correlation using linear regression analysis with a coefficient of determination of 80% between digital image processing output and sand circle measurements taken at the same spot was found. Thus, both concept and scientific principle were conclusively proven. A key finding was that separate regression models would have to be developed for each chipseal design type and possibly for each aggregate nominal size or chip grade.

1. Research background

1.1 Purpose of the research

The New Zealand seal design algorithm requires texture depth of the existing surface as a key input. Historically, texture has been measured using a volumetric technique called the sand circle test. This consists of spreading, with a straightedge in a circular motion, a known volume of uniform-sized sand on the road surface, measuring the diameter of the circular area covered by the sand, and dividing the volume (of sand) by the area to obtain an average texture depth. Even with experienced, skilled operators, the test takes some time to perform, and is normally done in live traffic conditions with varying levels of traffic control. Even though the reproducibility (40% error) of the sand circle test is poor, it is still the most common means to measure texture (Patrick et al. 2000).

With the development of laser technology, numerous attempts have been made to use lasers to measure texture (such as the Mini-Texture Meter and high-speed vehicle-mounted lasers used in New Zealand), but as these do not generate a volumetrics-based texture, laser-measured textures cannot be used for seal design. Multiple scanning lasers could feasibly generate volumetric texture, but this would be a very expensive procedure. Transit NZ has a stationary laser profilometer, which is a precise tool for measuring texture, but this device cannot be used for routine measurements of texture because of the substantial time and effort involved in setting up the device at each test site.

The purpose of this research was to evaluate whether a practical method of road surface texture measurement using digital image processing, incorporating information theory and fast Fourier transform (FFT) analysis could be developed. The objectives of the research were to develop:

- an accurate, repeatable method of measuring texture to replace the sand circle method,
- a fast, safe method of measuring texture to reduce the hazard of road surface texture measurement and minimise disruption to traffic.

Similar research has been undertaken in Texas, USA, but the focus of the American research was to correlate a qualitative performance rating of the chipsealed surface pavement with a quantitative measure of texture derived from digital imagery. The experiment was successful, and its results were published in the *International Journal of Pavement Engineering* (Gransberg et al. 2002). When a proposal was submitted to conduct experiments to correlate chipseal image FFT numbers to the measured skid resistance, the Texas highway agency was not interested in developing the concept any further. This research aims to apply the concept for measuring chipseal texture depth, for seal design purposes, in order to replace the present sand circle method of measuring texture in use in New Zealand.

Road users are rapidly becoming less tolerant of travel delays caused by road works, so the research will benefit road users by substantially reducing the time involved in measuring the texture of existing surfaces. Society in general is placing more emphasis on worker safety, and one of the potentially most dangerous activities on the road is the current manual measurement of surface texture using the sand circle test. The proposed research aims to significantly reduce exposure of field staff to the potential risk of injury and death while measuring surface texture.

1.2 Synopsis of research progress

The literature review for this project was completed, the software and hardware purchased and calibrated, the research methodology developed and field-tested in both New Zealand and the US, and preliminary data collection completed to validate the research methodology. These data consist of a series of corresponding digital images and sand circle tests which were correlated using linear regression analysis (Croakin & Tobias 2005). The results of the final research are documented in this report along with the preliminary work.

The interim report showed a statistical correlation based on the coefficient of determination (R^2) of 0.93 for the data obtained in the preliminary investigation. This was for digital image output measured by the sum of the FFT values in ring 3 of the images. The team was gratified to obtain such a strong correlation at such an early stage in the research, but nevertheless hoped to involve a larger proportion of the digital output. The images were 'sliced' into a large number of rings based on spatial frequencies. The waterfall graphs that were associated with each image visually indicated that the major variation between images of differing texture occurred in the first 25 rings. Thus, the research focused on that area of output and was able to obtain a statistical correlation based on the coefficient of determination (R^2) of 0.80. Even though the R^2 value is lower, this is a much more authoritative and representative correlation in that 25 times the information content of the image is used to correlate with the physical texture measurement. Thus, the research has conclusively proven that chipseal texture can generate a measurable mathematical relationship in a digital image.

2. Literature review

2.1 Review of chipseal design

New Zealand's chipseal design methodology is based on the theory and mechanisms first proposed by Hanson (1935), who related the bitumen application rate to the size of the stone chip, the ratio of the chip's average, least and greatest dimensions, and the residual void space within the single layer thickness of the aggregate cover. Later, the major assumptions were refined by McLeod (1974). Since then, the basic precepts have been refined by experience into a semi-empirical design procedure which provides corrections for existing surface texture and vehicle loading, culminating in the *Sealing Design Manual* (TNZ 1993).

One of the major difficulties in determining binder application rates is the non-uniformity of the existing pavement surface texture. Variation in the existing pavement occurs in both the transverse and longitudinal directions. The transverse variation is usually defined as the difference in the surface texture on the wheelpaths and outside/between the wheelpaths, including rutting. Longitudinal variation occurs as the surface condition varies along the road from areas where the underlying surface is oxidised to other areas where the surface may be smooth or bleeding.

2.1.1 Texture measurement

Surface texture refers to the macrotexture of the pavement surface (Austroads 2004). Surface texture is a measurement which influences the nominal size of aggregate used for the chipseal and thus ultimately determines material application rates, skid resistance, and road noise. Characterization of the pavement's surface texture is a critical step in the design process because non-uniform surface textures in both the transverse and longitudinal directions make it difficult to design a binder application rate.

Historically, the macrotexture has been measured using volumetric techniques, and the most common test procedure is the sand circle method. This method involves spreading 45 ml of sand (particle size of 300 μm to 600 μm) by revolving a straightedge until the sand is level with the tops of the cover aggregate (TNZ 1981). The volume of material that fills the surface voids determines the surface texture. The principle of this method is fairly straightforward: the greater the average texture depth, the greater the quantity of material lost in the surface voids. The average texture depth is calculated by dividing the volume of sand by the area of the sand patch (TNZ 1981), as shown in Figure 2.1.

$$\textit{Average Texture Depth} = \frac{57{,}300}{d^2} \ \textit{mm (d in mm)} \qquad \text{(Equation 2.1)}$$

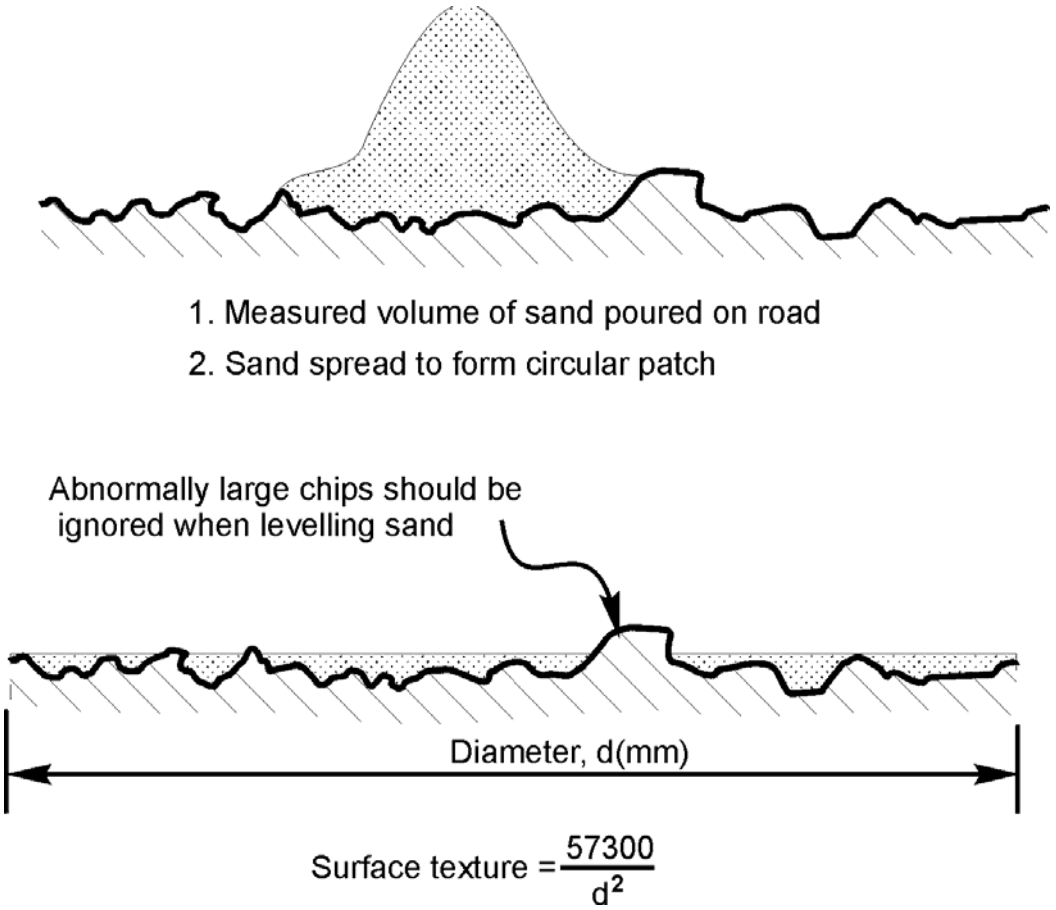

Figure 2.1 Sand circle test for texture measurement.

In New Zealand and Australia, two main variations in the sand circle method are used, either with a straightedge or a rubber-faced pestle. Across the two countries, the straightedge varies in length from 150 mm to 300 mm. The pestles differ from a brass disk with a rubber base with a measuring cylinder attached, to a rubber bung. The diameter of the face used to spread the filling medium ranges from 55 mm to 95 mm, with the 55 mm to 65 mm diameter being the most common (ARRB 2001). The British Standard BS 598:105:1990 "Sampling and examination of bituminous mixtures for roads and other paved areas: part 105 - methods of test for the determination of texture depth" requires the use of a rubber-faced pestle with a diameter of 65 mm including a 74 mm high by 29 mm-diameter measuring cylinder as a handle, with a total mass of 210 grams.

Several volumetric methods are used, such as ASTM Standard E-965 which uses glass spheres instead of sand, or another method used by NASA which uses grease. Another technique is the Circular Track Meter (CTMeter), which uses a laser to measure the profile of a circle 284 mm in diameter (892 mm in circumference) (ASTM 2003). The profile thus measured is divided into 8 segments of 111 mm each, and the average macrotexture depth is calculated for each of the segments of the circle. The final reported macrotexture for each test site is the average of all 8 segments. The textures measured using the CTMeter and sand circle method have been compared in a number of research projects, and the coefficient of determination (R^2) has been found to be between 0.94 and 0.92 (Henry 2000). Because the CTMeter uses lasers and electronics, this device should also

have better reproducibility than the sand circle test. However, even though the CTMeter has excellent correlation with the sand circle test, the CTMeter equipment is relatively expensive and the time required to do a CTMeter is substantially greater than the time required by an experienced operator to do a sand circle test. The CTMeter is not as cost effective as the sand circle test and actually increases the exposure of operators to vehicles and thus to the risk of injury while measuring texture.

In 2000-2001, Fulton Hogan conducted trials using three high frequency lasers mounted on a vehicle, in order to determine whether these 64 kHz lasers travelling at 50 km/h would be able to determine seal texture for use in seal design. The texture of the seals was measured over two years using the high frequency lasers. It was concluded that macrotexture could be derived from mean profile depth and possibly used to determine binder application rates but it was not financially viable to develop a dedicated high speed laser-based device for measuring texture (Vercoe 2002).

A photogrammetric technique was developed by Schonfeld of the Ontario (Canada) Ministry of Transportation, during the 1960s to 1980s. This technique involves measuring six parameters from stereo photographs of the seal:

- **asperity height** (measured from top of the background to the top of the projection),
- **asperity width** (the horizontal dimension of the projection, measured at the top of the background),
- **asperity edges** (describes the edges of the projection which come in contact with vehicle tyres),
- **asperity density or spacing** (estimated proportion of area populated with projections, compared with the background),
- **fine texture projection** (relative sharpness or roundness of the macro-projections); background fine texture projection (relative sharpness or roundness of the micro-projections in the background),
- **undrained cavities** (relative proportion of the depressions in the background surface) (Goodman et al. 2004).

The Schonfield method was originally done manually, which was extremely time-consuming, but even with modern computing power and image analysis software, is still a relatively time-consuming method of measuring texture. Quantifying the texture of a seal also depends on the type of seal being measured, so the different seal types are discussed in the next section.

2.1.2 Types of chipseals

Until recently, single chipseals were the most common type of seal. A single chipseal is constructed from a single application of binder followed by a single application of uniformly graded aggregate as shown in Figure 2.2. These are selected for normal situations where no special considerations would indicate that a special type of chipseal is warranted. It should be noted that the following figures are conceptual diagrams and that there are other variations on these designs that are in use in the field.

Figure 2.2 Single chipseal.

A double chipseal is constructed with two consecutive applications of both the bituminous binder and the uniformly graded aggregate as shown in Figure 2.3. The aggregate in the second application is typically about half the nominal size of the first application. Double chipseals have less traffic noise, provide additional waterproofing, and are a more robust seal in comparison with a single chipseal (Austroads 2004). They are utilised in high stress situations, such as areas that have a high percentage of truck traffic or on steep grades.

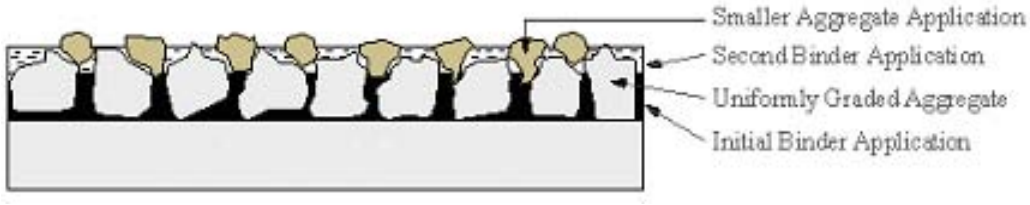

Figure 2.3 Double chipseal.

A racked-in seal is a special seal in which a single chipseal is temporarily protected from damage through the application of choke stone that becomes locked in the voids of the seal. The choke stone provides an interlock between the aggregate particles of the chipseal (Figure 2.4). The choke stone is used to prevent aggregate particles from dislodging before the binder is fully cured. These chipseals are in order in areas where a large amount of turning occurs to 'lock in' the larger pieces of aggregate with the smaller aggregate and prevent it from being dislodged before the seal is fully cured.

Figure 2.4 Racked-in seal.

Cape seals, named after the area in South Africa where they were invented, are basically a single chipseal followed by a slurry seal (Figure 2.5). The original South African technique was to use a larger than normal base stone (up to 20 mm). However, their application in other countries revolves around the use of a smaller size aggregate. Cape seals are very robust and provide a shear resistance comparable to that of asphalt (Austroads 2004).

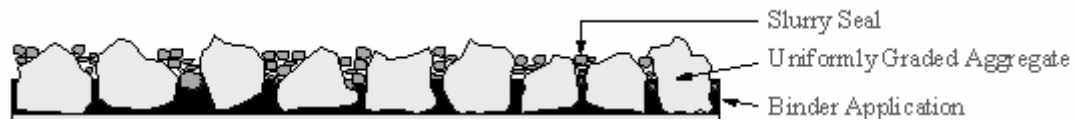

Figure 2.5 Cape seal.

Figure 2.6 shows how an inverted seal is constructed. It is called an inverted seal because the larger size aggregate goes on top of the smaller size aggregate and is therefore an inverted double seal. These seals are commonly used to repair/correct an existing surface that is bleeding, have been successfully used on bleeding surfaces with 30,000 AADT (annual average daily traffic) and are also used for restoring uniformity to surfaces with variation in transverse surface texture (Austroads 2004).

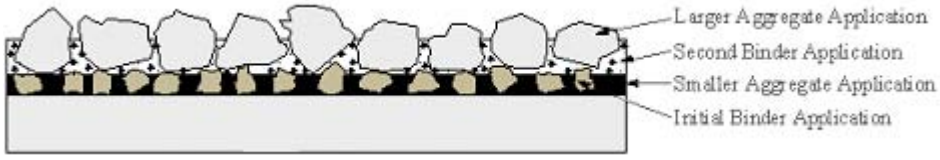

Figure 2.6 Inverted seal.

The sandwich seal shown in Figure 2.7 is a chipsealing technique that involves one binder application sandwiched between two separate aggregate applications.

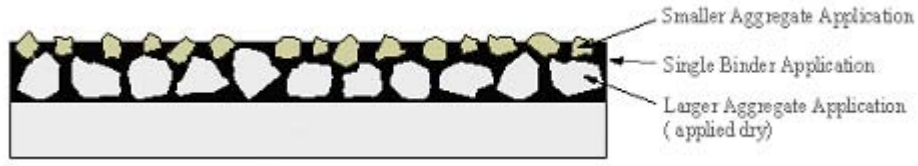

Figure 2.7 Sandwich seal.

Reinforcing a chipseal with geotextile products can enhance the performance of a conventional chipseal over extremely oxidised or cracked surfaces. The geotextile is carefully rolled over a tack coat, followed by a single chipseal being placed on top as in Figure 2.8.

Figure 2.8 Geotextile-reinforced seal.

The binder application rate is adjusted depending on the existing surface texture and it is necessary to decrease the binder application rate on surfaces that are exhibiting flushing or bleeding.

2.1.3 Performance classification of chipseals

Among the several distress types observed with chipseal surfaces, flushing and stripping are the most common (Benson & Galloway 1953, Holmgreen et al. 1985). Therefore, a quantitative measure of chip that seeks to measure chipseal surface texture performance should discern a satisfactory chipseal surface from a surface with either flushing or stripping distress. Flushing is characterised by the excessive embedment of aggregate into the asphalt binder and a loss of skid resistance that is caused by having the binder on the surface rather than the aggregate. In other words, a flushed surface has a smooth and slick appearance where the aggregates are less visible. Such distress is usually observed on the wheelpaths where repetitive loading by tyres causes subsequent embedment of aggregates. Flushing may be exacerbated by high binder application rates and by high surface temperatures.

Stripping, on the other hand, is the loss of aggregate from the pavement's surface. Such pavements have a very irregular appearance since the surface is not completely covered by the aggregate. This type of distress is generally observed on the centreline and between the wheelpaths of the pavement. Stripping occurs when the desired bond between the aggregate and binder fails. Low binder application rates, inadequate rolling, cool weather construction, and incompatible binder and aggregate types are common factors that might lead to stripping.

2.1.4 Performance specifications

Because of the extensive use of chipseals, New Zealand has moved away from the traditional prescriptive specification method used elsewhere to the use of performance specifications. The philosophy behind the Transit P/17 specification is that the texture depth after a twelve-month inspection is the most accurate indication of the performance of the chipseal for its remaining life. The specification contends:

> *the design life of a chipseal is reached when the texture depth drops below 0.9 mm on road surface areas supporting speeds greater than 70 km/h* (TNZ 2002).

The deterioration models developed for the P/17 specification require the minimum texture depth one year after the chipseal is completed using the following equation.

$$Td_1 = 0.07\ ALD \log Y_d + 0.9 \qquad \text{(Equation 2.2)}$$

where:

Td_1 = texture depth in one year (mm)
Y_d = design life in years
ALD = average least dimension of the aggregate

The entire specification is based on the assumption that chipseals fail as a result of flushing (bleeding) (TNZ 2002). Within the specification, road noise or aesthetic reasons are the only reasons for specifying a maximum texture depth. The final acceptance is based on the achievement of the required texture depth, without any significant chip loss. The test used to measure texture depth is therefore very important.

2.2 Digital image processing

The technique used in this research project was discovered on a chipseal research project funded by the Texas Department of Transportation (TxDOT). In that project, the researchers conducted site surveys of representative chipseal sections in each of the 25 TxDOT districts in conjunction with a state-wide chipseal constructability review (Gransberg et al. 1998). District personnel were asked to pick site survey sections that typified the overall quality of the chipseals in their districts. During each of these site surveys, the condition of the roadway was recorded by taking digital camera images to document the quality of pavement condition on each section. These images showed the overall condition of the roadway and close-up views of the shoulder, wheel path and the area between the wheelpaths. A standardised camera setup was used where the camera angle, zoom and height were kept constant in each of the images. Three of these images – shoulder, wheel path and between wheelpaths – were used to find an objective parameter that would quantify the quality level of the chipseal surface.

The parameter selected was the information content of each image as calculated by a mathematical transform to be discussed later in this report. In essence, each image has a finite amount of information contained within its boundaries. This information can be measured by determining the relative change in luminance intensity between adjoining pixels in the image. This relative difference in luminance is called the 'spatial frequency'. For example, if the luminance intensity of one pixel is high and the intensity of the next pixel is low, the difference between the pixels is a large number, and the two pixels would be said to have a high contrast and a correspondingly high spatial frequency. On the other hand, if two adjoining pixels have luminance intensities that are nearly equal, they would have low contrast and low spatial frequencies. High contrast occurs at the boundaries between two different objects in an image (Ellis 1976). The relative visibility of an object against its background is a function of the amount of contrast (Cuvalci et al. 1999). Figure 2.9 illustrates this concept graphically.

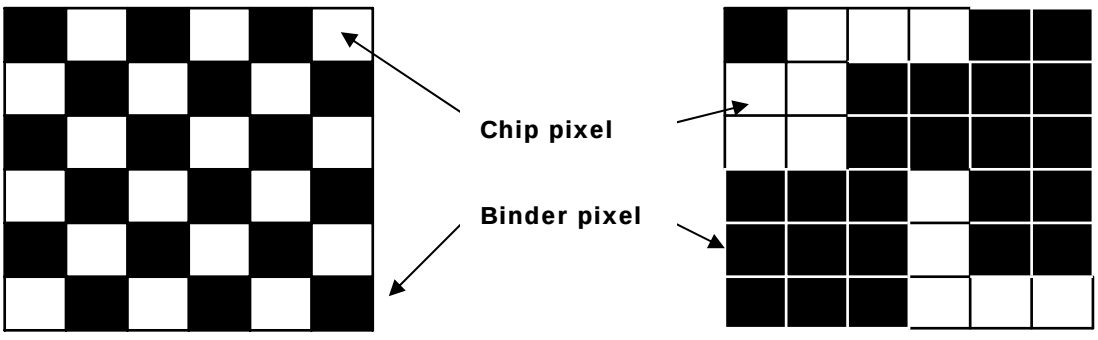

Figure 2.9 Information content measured as a function of contrast.

Thus, in the chipseal image, the contrast is formed by the amount of light reflected off the exposed aggregate against the amount of light reflected off the background formed by the asphaltic binder (Christie 1954). The Texas study found that TxDOT maintenance

personnel could easily distinguish between a satisfactory chipseal surface and an unsatisfactory one by visual inspection (Gransberg et al. 1998). It was also obvious to the naked eye that the difference between chipseal performance success and failure had to do with the relationship between the aggregate and the surrounding binder. Therefore, it was postulated that one could measure the surface condition by correlating the information content of a digital image and the qualitative rating of the human expert. Such a quantitative measure would significantly facilitate the decision-making process of allocating funds among several chipseal candidate sections on a basis of a quantitative comparison rather than qualitative comparison.

The Image Processing Toolbox of MATLAB® software (MATLAB® 1997, Tang 1999) was utilised to process the digital images of chipseal test sections in Texas. The processing of the chipseal images consisted of filtering the information content found in the images and quantifying this filtered information. One way to filter information in such an image is to detect the edges of the aggregate particles (i.e. focusing on the boundary between the aggregate and the surrounding binder). As will be seen later, the edge patterns of flushed, stripped and satisfactory pavement surfaces exhibit a significant difference. This difference in edge patterns constituted the main analysis tool to differentiate a flushed or stripped surface from a satisfactory pavement. When a sufficiently large population is imaged and its qualitative performance rating is associated with the product of the FFT image processing output, a distinct difference can be seen between chipseal surfaces with satisfactory texture and those that have failed either by flushing or shelling. Figure 2.10 comes from the previously mentioned article that reported this concept (Gransberg et al. 2002). One can easily see the potential for associating a quantitative rather than qualitative texture rating and being able to regress the relationship between the physical texture measurement and its associated image processing output to derive a formula that would allow the engineer to compute the texture measurement from the image output. Thus, the literature and mathematical justification for this proposed methodology must be reviewed and explained to give the reader the necessary background before moving on to the details of the current research.

2.2.1 Mathematical background to the fast Fourier transform

As previously stated, the mathematical process that will be used in this research is called the fast Fourier transform (FFT). This approach can easily be used to quantify the information content of a digital image using a very straightforward application of information theory (Cuvalci et al. 1999). The proposed approach is quite elegant in that it seeks to measure the information content of an image and then use that quantitative measure to statistically correlate with a physical texture measurement taken at the same location as the image. Thus, it quite intuitively seeks to differentiate surface texture on a basis of visual information content. As a result, the process contains a built-in check on image processing output: the ability to qualitatively confirm that images of like visual texture (i.e. satisfactory, flushed, etc.) are also yielding similar FFT numbers as well as similar sand circle measurements. The literature on the FFT explains its use in this particular project.

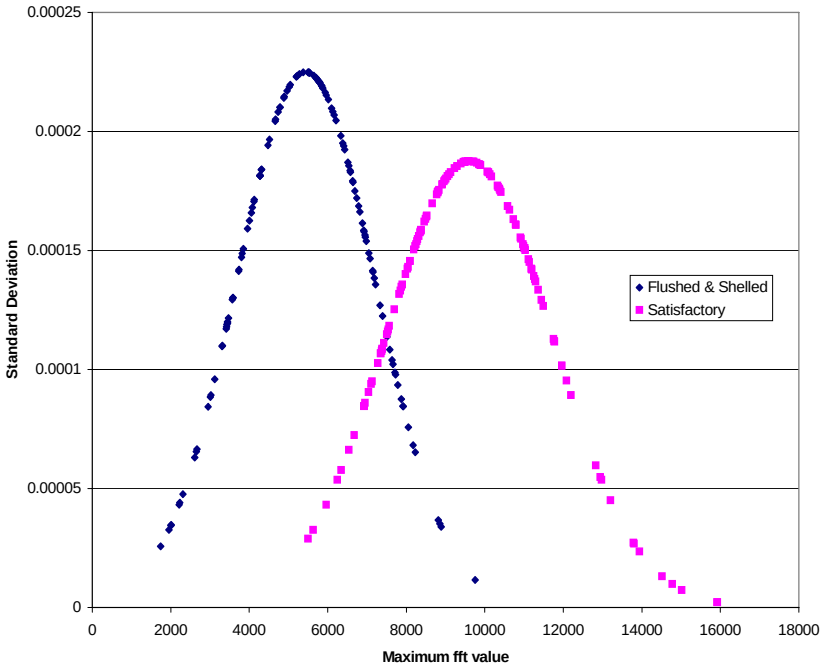

Figure 2.10 Normal distribution of maximum FFT values for different textures (Gransberg et al. 2002).

2.2.1.1 Fourier series

Fourier analysis was initially developed by the physicist Joseph Fourier to study heat transfer problems (Goodman 1968, Wilson 1995, Hecht 1975) where it was recognised that any function, $f_p(x)$, whose graph displays a periodicity, T, can be considered to be an infinite sum of sinusoidal functions. The Fourier series may be represented as the sum of a series of sine functions, cosine functions, complex exponential functions or any of several other sinusoidal representations (Wilson 1995).

2.2.1.2 Fourier series representation of a limited function

A uniform and finite periodic function $f_p(x)$ with period, p, is defined over a range of its variable x between x_0 and x_1. This function may be represented as follows at any point over its range by a series of circular functions where n is an integer.

$$p = x_1 - x_0, \qquad \text{and} \qquad \omega = \frac{2\pi}{p} \qquad \text{(Equation 2.3)}$$

$$f_p(x) = \frac{A_0}{2} + \sum_{n=1}^{\infty} (A_n \cos(n\omega x) + B_n \sin(n\omega x)) \qquad \text{(Equation 2.4)}$$

$$A_0 = \frac{2}{p}\int_{x_0}^{x_1} f_p(x)dx, \quad A_n = \frac{2}{p}\int_{x_0}^{x_1} f_p(x)\cos(n\omega x)dx, \quad B_n = \frac{2}{p}\int_{x_0}^{x_1} f_p(x)\sin(n\omega x)dx$$

(Equation 2.5)

$$f_p(x) = \sum_{n=0}^{\infty} C_n \cos(n\omega x - \theta_n) \qquad \text{(Equation 2.6)}$$

$$f_p(x) = \sum_{n=-\infty}^{\infty} D_n e^{in\omega x} \;,\; D_n = \frac{1}{p}\int_{x_0}^{x_1} f_p(x) e^{-in\omega x} dx \qquad \text{(Equation 2.7)}$$

Where: x is an x-unit (in spatial case it should be a length unit)

ω is an angular frequency in radiance per x-unit

θ_n, is a phase shift angle

A_n B_n C_n & D_n are amplitudes of the frequencies at $\omega_n = n\omega x$

Figure 2.11 shows a MATLAB® generated waveform, $f_p(x) = \sin 2\pi x$, with its corresponding spectrum. The period of $f_p(x)$ is p = 1 LU (length unit) and the frequency $f = \frac{1}{p} = 1$ LU^{-1} or angular frequency $\omega = \frac{2\pi}{p} = 2\pi \frac{rad}{LU}$ and $b_1 = 1$ represent the only non zero component in the spectrum.

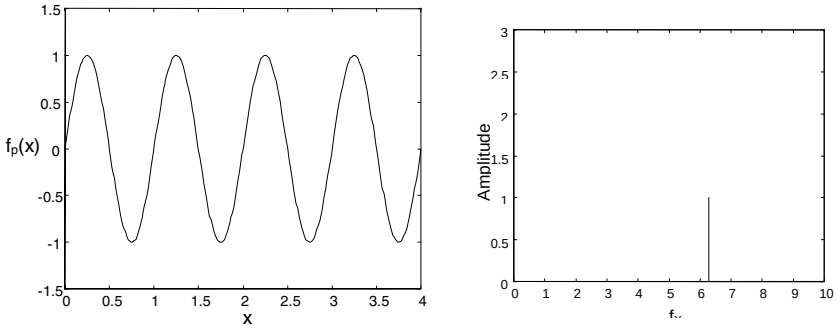

Figure 2.11 A single frequency wave ($f_p(x) = \sin 2\pi x$), and its spectrum.

2.2.1.3 Spatial and time domain of Fourier series

The Fourier series of any periodic function may be represented in the x-domain (either spatial or time domain) as a function of f(x) or in the ω-domain as a function of frequency F(ω).

$$f_p(x) = \sum_{n=0}^{\infty} F_n(\omega) \qquad \text{(Equation 2.8)}$$

When the function is represented in x-space it is usually a reasonably continuous function in x. In ω-space, the function is represented as an infinite series of amplitudes, A_n, B_n, C_n, or D_n, at discrete frequencies, ω_n , with discrete phase shifts θ_n. The discrete frequencies are determined only by the period, T, of the periodic function. Each frequency contains a portion of the total energy or power in the function f(x). The total energy in the function f(x) is the sum of the amplitudes in each discrete frequency.

$$E_{f(x)} = \sum_{n=0}^{\infty} |C_n|^2 \text{ , or, } E_{f(x)} = \sum_{n=-\infty}^{\infty} \left|D_n e^{i(n\omega x + \theta_n)}\right|^2 = \sum_{n=-\infty}^{\infty} |D_n|^2 \qquad \text{(Equation 2.9)}$$

The Fourier series moves a function back and forth between dual domains, frequency domain, ω, and position domain, x, with different aspects of the function represented uniquely in each domain. It has been noted that Fourier series of periodic functions have discrete frequency content and an infinite sum of the discrete frequencies. The discrete frequencies are associated with the period as the following:

ω_n = n2 π /T; n= 0, 1, 2, 3,…
ω_0 = 0×2 π /T; constant term, the non-oscillating term,
ω_1 = 1×2 π /T; the fundamental frequency, first oscillating term
ω_2 = 2×2 π /T; the first harmonic, second oscillating term
ω_3 = 3×2 π /T; the second harmonic, third oscillating term

As the period *T*, decreases, ω_1 becomes larger and (ω_2 - ω_1) grows larger, the distance between ω_{n+1} and ω_n increases. As the period *T,* increases, ω_1 becomes smaller and ω_1 and ω_2 grow closer together. As *T* becomes very large, ω_1 and ω_2 move close together until, as *T* goes to infinity, the frequency becomes continuous. We have a non-periodic, f(*x*), in the space domain and a continuous function F(ω), in the frequency domain. This leads us to a tool known as *Fourier analysis*.

2.2.1.4 Fourier analysis in one dimension

Any function, $f(x)$ (not limited to periodic function), may be considered to be composed of the superposition of a series of continuous periodic functions of suitable amplitudes and frequencies. A periodic function, u, can be represented by $F(u)e^{jxu}$, so that the original function, considered as a summation of periodic functions, becomes the following:

$$f(x) = \int_{-\infty}^{\infty} F(u)e^{jxu}du\,, \quad F(u) = \frac{1}{2\pi}\int_{-\infty}^{\infty} f(x)e^{-jxu}dx \qquad \text{(Equation 2.10)}$$

The function, which gives the amplitudes *F(u)* of the periodic terms of frequency u, is called the Fourier transform equation. Whenever *f(x)* or *F(u)* can be determined, the other can be computed from the Fourier transform relationship. This concept is of extraordinary power and is used in many problems of analysis in optics.

Since the Fourier transform *F(u)* is a frequency domain representation of a function *f(x)*, the *u* characterises the frequency of the decomposed cosinusoids and sinusoids and is equal to the number of cycles per unit of *x* (Bracewell 1965). If a function or waveform is not periodic, then the Fourier transform of the function will be a continuous function of frequency (Brigham 1974).

2.2.1.5 Discrete Fourier transform

As computers work only with discrete data, numerical computation of the Fourier transform of *f(x)* requires discrete sample values of *f(x).* Then, the computer can compute the transform *F(u)* only at discrete values of *u*. For example, a continuous function *f (x)* is discretised into a sequence by taking N samples Δx units apart.

$$\{f(x_0), f(x_0+\Delta x), f(x_0+2\Delta x), \mathrm{K}\ , f(x_0+[N-1]\Delta x)\} \qquad \text{(Equation 2.11)}$$

It will be convenient in subsequent developments to use *x* as either a discrete or continuous variable, depending on the context of the discussion.

$$f(x) = f(x_0 + x\Delta x) \qquad \text{(Equation 2.12)}$$

Where x now assumes the discrete values 0, 1, 2, ,$N-1$. .

In other words, the sequence $\{f(0), f(1), f(2), , f(N-1)\}$ denotes any N uniformly spaced samples from a corresponding continuous function. With this in mind, the discrete Fourier transform pair that applies to sampled function is given by the following equation:

$$F(u) = \frac{1}{N}\sum_{x=0}^{N-1} f(x)\exp[-j2\pi ux/N] \qquad \text{(Equation 2.13)}$$

for u = 0, 1, 2,....., N − 1, and

$$f(x) = \sum_{u=0}^{N-1} F(u)\exp[j2\pi ux/N] \qquad \text{(Equation 2.14)}$$

for x = 0, 1, 2,....., N − 1.
In the two-variable case the discrete Fourier transform pair is:

$$F(u,v) = \frac{1}{MN}\sum_{x=0}^{M-1}\sum_{y=0}^{N-1} f(x,y)\exp[-j2\pi(ux/M + vy/N] \qquad \text{(Equation 2.15)}$$

foru = 0, 1, 2,....., $M-1$, v = 0, 1, 2,.....N − 1, and

$$f(x,y) = \sum_{u=0}^{M-1}\sum_{v=0}^{N-1} F(u,v)\exp[j2\pi(ux/M + vy/N] \qquad \text{(Equation 2.16)}$$

for x = 0, 1, 2,.....,. $M-1$, y = 0, 1, 2,.....N − 1.

The above equations can be used to compute transforms and inverse transforms of appropriately sampled data. The discrete Fourier transform and its inverse are periodic with period N - only the N values of each variable in any one period are required to obtain $f(x, y)$ from $F(u, v)$. In other words, only one period of the transform is necessary to specify $F(u, v)$ completely in the frequency domain. In the one-variable case, for example, because of translation property of discrete Fourier transforms, the magnitudes of the transform values from $(N/2)+1$ to N − 1 are reflections of the values in the half period to the left of the origin (the actual highest frequency is $N/2$).

2.2.1.6 Fast Fourier transform

The fast Fourier transform, FFT, is designed to minimise computer time. The number of complex multiplications and additions required to implement certain equations is proportional to N^2. Proper decomposition of this equation can make the number of multiplication and addition operations proportional to $N \log_2 N$. The decomposition procedure is called the *fast Fourier transform* (FFT) *algorithm*. The reduction in proportionality from N^2 to $N \log_2 N$ operations represents significant savings in computational effort.

2.2.2 Information theory

Information theory is used to quantify the information content, which can be measured in a given image based on the luminance in the pixels. Simply put, any given image contains a finite amount of information. A component of that information is displayed by the level of reflected luminance present in each pixel. When one compares the measured value of reflected luminance in a given pixel to the luminance values in each of the pixels that surround it, the difference is the quantity of information. Thus, if the change from one pixel to another is zero (i.e. the first pixel is white and the next is also white), then no change in information occurs. Conversely, if the difference in reflected luminance is high (i.e. the first pixel is white and the next is black), then a large change in information occurs. This change in information content is conveyed through the amount of contrast that is displayed in the image.

Thus, to apply this theory to measuring chipseal texture, one needs only to quantify the amount of contrast in an image of a surface that has a satisfactory texture and compare that to the amount of contrast in one that is unsatisfactory. Intuitively, an image of a surface that displays severe flushing will have very little contrast because the aggregate will have been forced down into the binder and most of the surface will be the reflected luminance of the binder yielding very little information change between pixels. In an image of satisfactory chipseal texture, the aggregate will be clearly visible and the binder will furnish the background and yield a substantial amount of information change as the process moves pixel by pixel across the image.

2.2.2.1 Fourier analysis of digital images (frequency domain)

The Fourier transform decomposes a waveform (or function) into sinusoids of different frequencies that sum to the original waveform. It identifies or distinguishes the different frequency sinusoids and their respective amplitudes (Brigham 1974). Physical laws suggest that any conceivable object that can yield an image may always be represented by a series or by a simple or multiple Fourier integral. The amplitudes of the terms of the series or the integrand of the integral can usually be regarded as describing the spatial frequencies, which leads to a complete representation of the same object in a different domain rather than the spatial.

This idea is utilised in contemporary optics and mathematics. It is often useful to think of functions and their transforms as occupying two domains. These domains are referred to as the upper and the lower domains in older texts, "as if functions circulated at ground level and their transforms in the underworld" (Bracewell 1965). They are also referred to as the function and transform domains, but in most physics applications, they are called the time and frequency domains respectively. Operations performed in one domain have corresponding operations in the other. For example, the convolution operation in the time domain becomes a multiplication operation in the frequency domain, and the inverse is also true. Such theorems allow one to move between domains so that operations can be performed where they are easiest or most advantageous. The earlier contents of this chapter prepare us for the most often used transform in our research, the two-dimensional FFT on a discrete matrix (the digital image). The result of this transform is a

discrete matrix whose elements represent the frequency domain amplitudes (Bracewell 1965).

2.2.2.2 Fourier transform model using MATLAB®

The MATLAB® computer software provides the functions to perform a two-dimensional discrete Fourier transform (FFT2) and its inverse (IFFT2) (Goodman 1968, Wilson 1995, Meyer-Arendt 1972). A picture is stored in a MATLAB® readable format: .jpg, .tiff, .gif (in pixels). The FFT2 converts the bitmap into its frequency space counterpart. The command FFT2 transforms the real space 2-D matrix into a complex 2-D matrix. The matrix has two parts: the real part of each element (modulus) and the magnitude of that modulus which is equivalent to the power spectrum or spatial energy content of the image. The magnitude of the modulus is the most often used representation of the frequency spectrum of an image. The phase portion is necessary for accurate image reconstruction but not for spatial frequency analysis.

It is common to illustrate Fourier spectra of images as intensity functions. The dynamic range of Fourier spectra is usually much higher than the typical display method is able to reproduce. An observer can view that on a computer monitor, in which case only the brightest (largest values) parts of the spectra are visible on the display screen (see Figure 2.12).

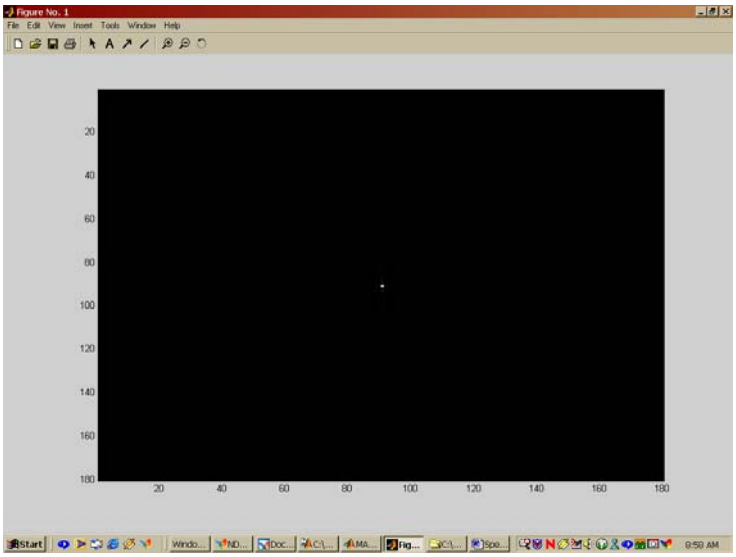

Figure 2.12 Visible spectra of FFT on a computer display.

A useful technique that compensates for the difficulty shown in Figure 2.12 consists of displaying the following function instead of $|F(u,v)|$, where c is a scaling constant and the logarithm function performs the desired compression.

$$D(u,v) = c\log[1+|F(u,v)|] \qquad \text{(Equation 2.17)}$$

The use of this equation greatly facilitates visual analysis of Fourier spectra, shown in Figure 2.13, as a 2-D intensity illustration of the log-scaled Fourier spectrum. The intensity illustration replaces the perspective view of the 3-D graph with a top view using colour intensity or grey scales for amplitudes. The large central amplitude is equivalent to the average background luminance of the image. The surrounding low frequency amplitudes are large and the amplitudes of the higher frequencies of the Fourier transform drop off rapidly.

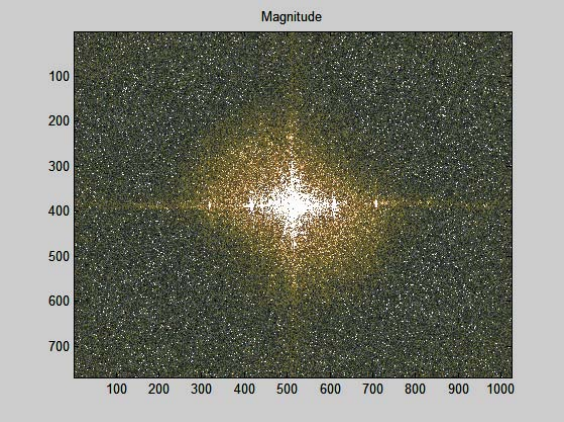

Figure 2.13 Magnitude portion of the FFT of an image.

If plotted in its intensity form, there is:

- an extremely tall spike representing the "zeroth" term of the discrete Fourier transform (DC component) at the centre of the frequency plane,
- the low-frequency and mid-frequency range in which one finds usually lower amplitude spikes,
- the high frequency range, with very low amplitude spikes.

Usually in the high-frequency range, the amplitude of the frequency components are relatively flat. However, for images with highly periodic features, there are features shown in the high frequency range.

2.2.2.3 The FFT algorithm

The algorithm used to obtain this spatial information from a digital image operates as follows:

- The image is acquired using a CCD (charge coupled device) camera. The CCD camera is chosen for the unique properties it provides.
- The acquired image is converted into a black and white image, which contains the standard range of 256 grey levels.
- The image is processed and the FFT of the image is computed.
- The frequency components in the FFT are segregated as shown in Figures 2.14 and 2.15. This segregation is achieved by separating the FFT into bands (regions). The frequency components start with the zeroth component in the centre pixel (Stemprok et al. 2000).

- The sum of the FFTs of the pixels local to each ring is calculated.
- The sums are plotted against the frequency band using any graphing software package.
- The data is ready for analysis.

2.2.2.4 Frequency bands

Figures 2.14 and 2.15 graphically illustrate the process of parsing the digital image into frequency bands. Choosing the thickness of the frequency band is critical to the exercise of spatial content analysis, as this method separates the FFT frequency components. The distribution of different frequency components can be uniformly spaced throughout the FFT image array, or can be non-linearly distributed from the centre, radiating outwards. Care should be taken in determining the optimal size of the frequency band to obtain correct results.

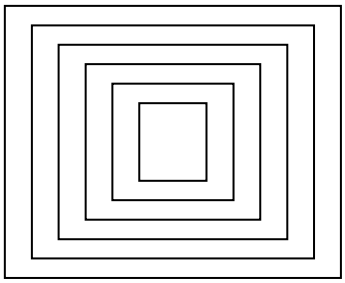

Figure 2.14 Rectangular frequency bands.

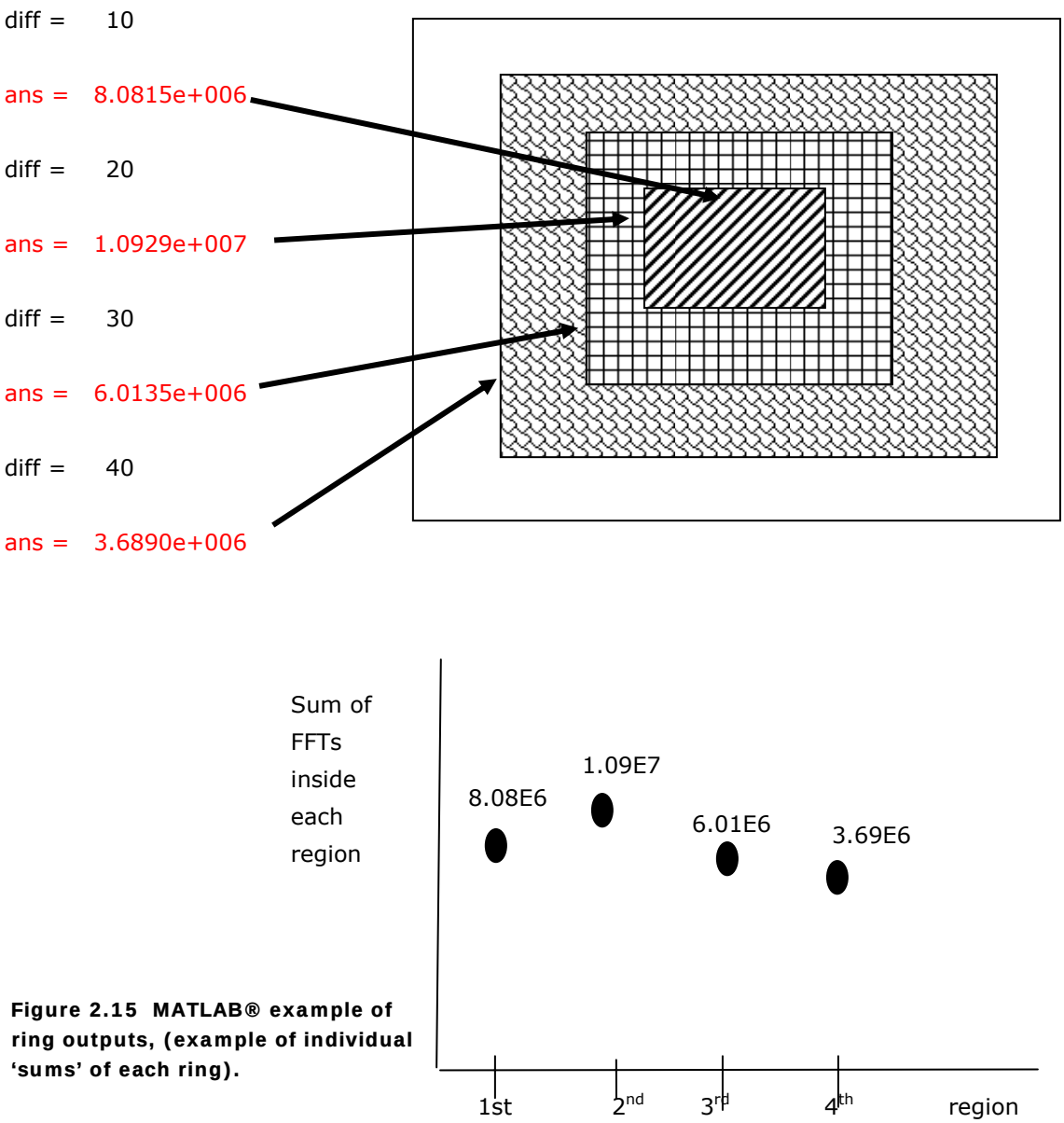

Figure 2.15 MATLAB® example of ring outputs, (example of individual 'sums' of each ring).

When choosing the frequency band division, the two choices are: circular division and rectangular division (Stemprok et al. 2000). The FFT computed by the software is in the form of a matrix. Thus, it creates a two-dimensional array for a two-dimensional image. Because of this spatial compatibility, the rectangular division furnishes a format that facilitates the writing of image-processing code and makes subsequent computations straightforward. To make a circular division, one must locate the centre of the matrix and calculate the distance between this centre and each element of the matrix. Each pixel element must be specified as belong to group "n" instead of group "n+1", which means more computing for circular division. Thus, it is more complex and does not seem to enhance accuracy. Therefore it has been found that a rectangular division method is sufficient for our purposes (Stemprok et al. 2000).

2.2.2.5 Imaging 'theory'

Examining the equations of a 2-D discrete Fourier transform, it is obvious that the luminance is related to a zeroth term of Fourier analysis. The computer code separates the zeroth term, also called the DC component. The centre of the frequency domain should be the result of summing all the grey-level values of every pixel in the picture. The DC component describes how bright the picture looks from a distance. The DC component does not describe any feature of the picture that is detailed. The electrical term ('DC component') refers to its steady value.

Usually when a large-size picture is involved, this DC component tends to get extremely large compared to other frequency components in the image. Even though its value can be much larger than the other frequency components, this aspect does not get in the way of examining other potentially useful values. The first band calculation puts the DC component along with other low frequency components (centre block - the first band) and finds its summation. To avoid the effect of this DC component it is possible to remove the centre block of the divisions. It is believed that the DC component of the transform should be separated from the matrix because it has a special property. It describes the background luminance that tells relatively how bright one image is among a series of such images (Stemprok et al. 2000). The MATLAB® software puts the DC component of the transform on one of the four centremost locations. That has to be properly considered by the software.

Defining the frequency range is not trivial, and it is currently under development. In the high frequency range, noise usually takes up most of the activity instead of the real image information. The following set of figures illustrates how the current technology is applied to an image of a cow. This image is selected as it furnishes a clear visual target around which the reader can visually discern the various steps in the image-processing algorithm. An FFT image was calculated, then the FFT was filtered using a low and high pass filter in MATLAB®. Figures 2.16 and 2.17 display the image when passed through the low pass and the high pass filter.

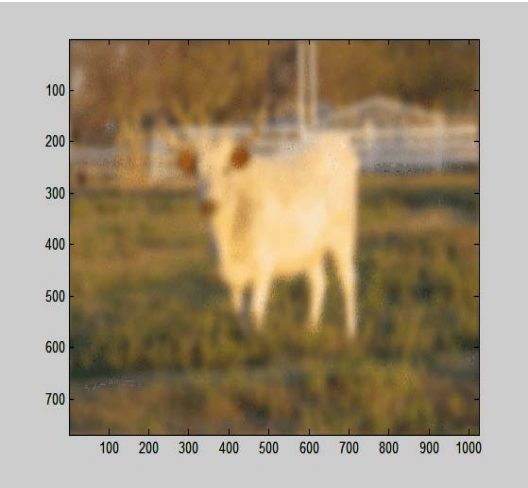

Figure 2.16 Image of cow as displayed in MATLAB® when passed through a high pass filter (frequency bands 25-64).

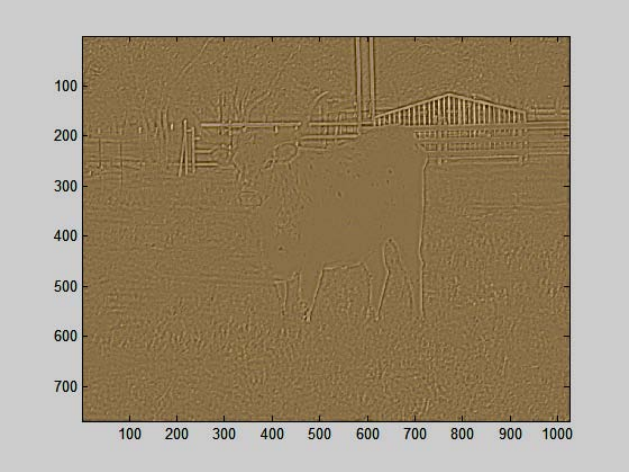

Figure 2.17 Image of cow as displayed in MATLAB® when passed through a high-pass filter (frequency bands 25-64).

In Figure 2.16 the image was passed through a low pass filter; the image was clearly visible, but the image is blurred and the finer details of the image are not available. In Figure 2.17 when the image was passed into a high pass filter, it is seen that no blur occurs in the image and the sharp edges and the transitions in the image are clearly visible. In order to know the finer details in the image in the high frequency band, the image is enhanced. Figure 2.18 shows the image from the high pass filter, which is enhanced in order to view the image clearly.

Figure 2.18 Enhanced image from the high pass filter.

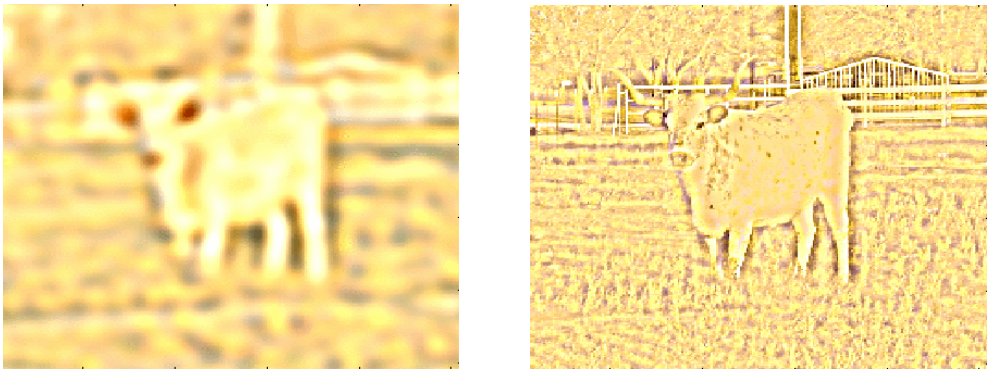

(a) (b)

Figure 2.19 Enhanced image from the high pass filter two times: (a) frequency bands 25-45 (b) frequency bands 45-64.

The high pass frequency band was divided into two different bands, the first consisting of the frequency bands from 25-45 and the other consisting of the frequency bands from 45-64. Figure 2.19 shows the image from the high pass filter, which is enhanced two times in the two different bands. Figure 2.20 shows the image obtained after enhancing the FFT pixel values three times. Figure 2.19 shows that the sharper and the finer details of the image are observed in the frequency bands 45-64.

From Figure 2.20 the frequency bands above 45 are shown to give information regarding the sharp edges in the image. The frequency bands from 25-45 give information regarding the contrast in the image. From the filtered images it could be inferred that the low frequency components (smooth variations) constitute the base of an image, and the high frequency components (the edges which produce the detail) refine the image. Low pass filtering involves the elimination of high frequency components in the image and results in blurring of the image (a reduction in sharp transitions associated with noise). An ideal low pass filter would retain all low frequency components, and eliminate all high frequency components.

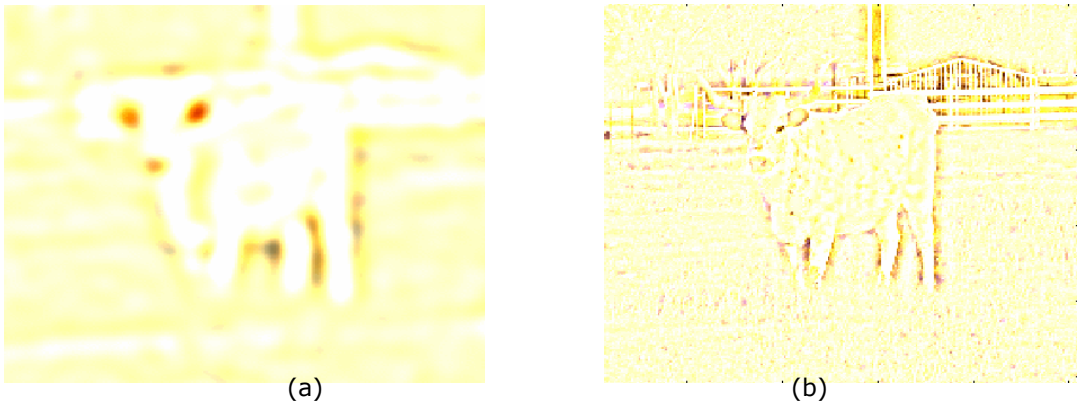

(a) (b)

Figure 2.20 Enhanced image from the high pass filter three times: (a) frequency bands 25-45 (b) frequency bands 45-64.

Edges and sharp transitions in colour in an image contribute significantly to high-frequency content of its Fourier transform. When the image is passed through a high pass filter from Figure 2.16 only the sharp edges in the image are visible. The high frequency component in the Fourier transform constitutes the finer details available in the picture. When an image is passed through an ideal high pass filter, which removes all the low frequency components, the actual details of the object, which are invisible to the eye, can be viewed.

2.2.2.6 Sampling theorem

A band-limited signal is a signal $f(t)$, which has no spectral components beyond a frequency B in hertz (Hz) (Bose 2004, Hanselman & Littlefield 2001).

$$F(s) = 0 \text{ for } |s| > B \qquad \text{(Equation 2.18)}$$

The sampling theorem states that a real signal, $f(t)$, which is band-limited to B in Hz can be reconstructed without error from samples taken uniformly at a rate R > 2B samples per second. This minimum sampling frequency, R_N= 2B Hz, is called the Nyquist rate (Nyquist frequency). The corresponding sampling interval, T = 1/2B (where t = nT), is called the Nyquist interval. A signal band limited to B Hz that is sampled at less than the Nyquist frequency of 2B, i.e. which was sampled at an interval T > 1/2B, is undersampled (Ifeachor & Jervis 2002, Bose 2004). That causes a problem in signal reconstruction.

2.2.2.7 CCD imaging for FFT processing

It should be noted that daylight pictures have a horizontal illuminance of 60,000 Lux, whereas night images have a minimum of 10 Lux and a maximum of 50 Lux. Thus, the mathematical relationship that defines contrast is easier to achieve at night. For example, if an LED forming a target image was turned on and imaged at night, it can be clearly seen because of the contrast between the LED and unlit background. This is because the illuminance caused by an LED is about 5000-million candela that is in the same order of magnitude with the night time environment. However in the daylight picture when the environment is much brighter, the LED can not be seen at all. This is because the camera divides the luminance into 256 levels from brightest to dimmest for each image. The day and night images are different in scale by 3 orders of magnitude. So it is necessary to adjust the relative amplitudes of the day and night images to place them on the same scale (Stemprok et al. 2000). The daylight images are shown fully in the photopic region of vision while the roadway lighting image is in the mesoptic region. The 3 orders of magnitude difference makes the night time image irresolvable with respect to the daylight image if they are on the same scale.

In order to be comparable, the standardised image acquisition method should be carefully designed and carried out. To do so, the experiment must maintain fixed focal length, and fixed tilt of camera. When these constraints are met, constant lighting is not needed because the camera self-adjusts (Stemprok et al. 2000).

3. Research methodology

The research methodology on this project consists of the following stages:

1. **Procure and adapt software and associated hardware to process digital images of seals**: A copy of MATLAB® with the Image Processing Toolbox was purchased and customised to process the digital images, along with the necessary hardware and expanded digital storage capacity.
2. **Trial software on sample photographs**: A small number of sample photographs were taken of actual seals and processed to verify that the image processing worked properly. The texture of the seals was measured with the sand circle test. The processed image output was related to the sand circle measurements using qualitative ratings of the surface condition to ensure that the study could replicate the results of the literature with the current hardware and software.
3. **Peer review of trial**: Before commencing the next stages, the peer reviewers evaluated the outcomes thus far. The review included an assessment of the feasibility of developing a workable system for measuring the texture of seals with sufficient accuracy for use in seal design. Comments were incorporated as appropriate into the next stage of the trials.
4. **Develop prototype for field trials**: A standard experimental setup was developed and refined to ensure that all images were collected in a scientific manner that can be easily replicated. Images were made with a digital camera. The distance above the surface, and aspect in relation to the horizontal plane were standardised to ensure uniformity in the images. Specific trials were undertaken to ensure that the images could be replicated with a high degree of reproducibility. Issues regarding the ability of the self-adjusting digital camera to regulate the amount of light in each image were also addressed to confirm the findings in literature on this issue.
5. **Field trials of prototype**: Data collection primarily involved collecting images of a representative sample and range of New Zealand chipseals. The variables included chip size, types of seal (single or double, racked-in, etc.), and age of seal. The texture of the seal captured in each image was measured using the sand circle test. Additionally, any general distress condition such as flushing/bleeding or stripping/ravelling was noted. The images collected in New Zealand were processed through a computer program that quantifies the information contained in each image using information theory. Essentially, the software compares the reflected luminance presented in each pixel with the luminance of the pixels that surround it.
6. **Mathematical analysis of collected data**: The outputs from the image analysis and the sand circle test were tested using linear regression techniques to determine if a physical relationship could be identified between the two. The primary measure used to establish mathematical trend was the coefficient of determination (R^2 value) calculated from the curve fitting conducted during the regression analysis. The imagery output was separated by ring as described in Section 2.2.2.3. Each ring's FFT summation was compared to its corresponding sand circle measurement and calculated average texture depth to determine if a strong correlation existed.

Additionally, groups of ring FFT values were aggregated and compared in the same fashion.

7. **Prepare draft final report**: When the mathematical analysis of the data was complete, this final research report was prepared to document the research, discuss the results observed in the study, and report conclusions that flow out of the analysis.

3.1 Procure, adapt, and calibrate software and hardware

A copy of MATLAB® software with the Image Processing Toolbox was purchased and customised to process the digital images, along with the necessary hardware and expanded digital storage capacity. A Sony Mavica digital camera and a tripod with three levelling bubbles were procured and used to collect chipseal image data. The Sony Mavica model MVC-FD75 uses a 4.5 mm CCD, with auto exposure and auto white balance.

Digital images from the Texas research project (Gransberg et al. 1998) were used to test the adapted software to ensure that a similar numeric result to the ones published in Gransberg et al. (2002) could be achieved with the new hardware and new software. These limited tests were successful. The previous protocol was revised to take advantage of new imaging processing features as well as current research that produces a more robust output data set. The new protocol is based on evaluating FFT output from the first 25 rings (see Figures 2.14 and 2.15) rather than a single maximum special frequency of the FFT output in pixels (see Figure 2.13). Thus, the output can be displayed as a waterfall graph (Figure 3.1) rather than the histogram used in the Texas study (Figure 3.2). This allowed the researchers to optimise the regression analysis with respect to frequency band and greatly enhance the probability that regression coefficients of determination could be found that will improve the accuracy of the texture measurement predicted by the computed FFT in a given chipseal image.

To calibrate the experimental equipment, a four-week trial and calibration regimen was undertaken in the US, collecting and processing digital images of chipseal surfaces in Oklahoma. The following experimental requirements were determined:

- The optimum lens height was found: 0.80 - 0.85 m above surface.
- Maximum tolerance for tilt from vertical was found: 5 degrees from vertical.
- The optimum image size was found: optimum image size is at maximum zoom setting on camera at optimum lens height.
- The experimental set up was tested and found to be easily replicated with little or no change in calculated image information content between different operators.
- The camera's ability to satisfactorily self-adjust to varying amounts of natural daylight and that specific image illumination did not need to be standardised were verified, as predicted in the literature.

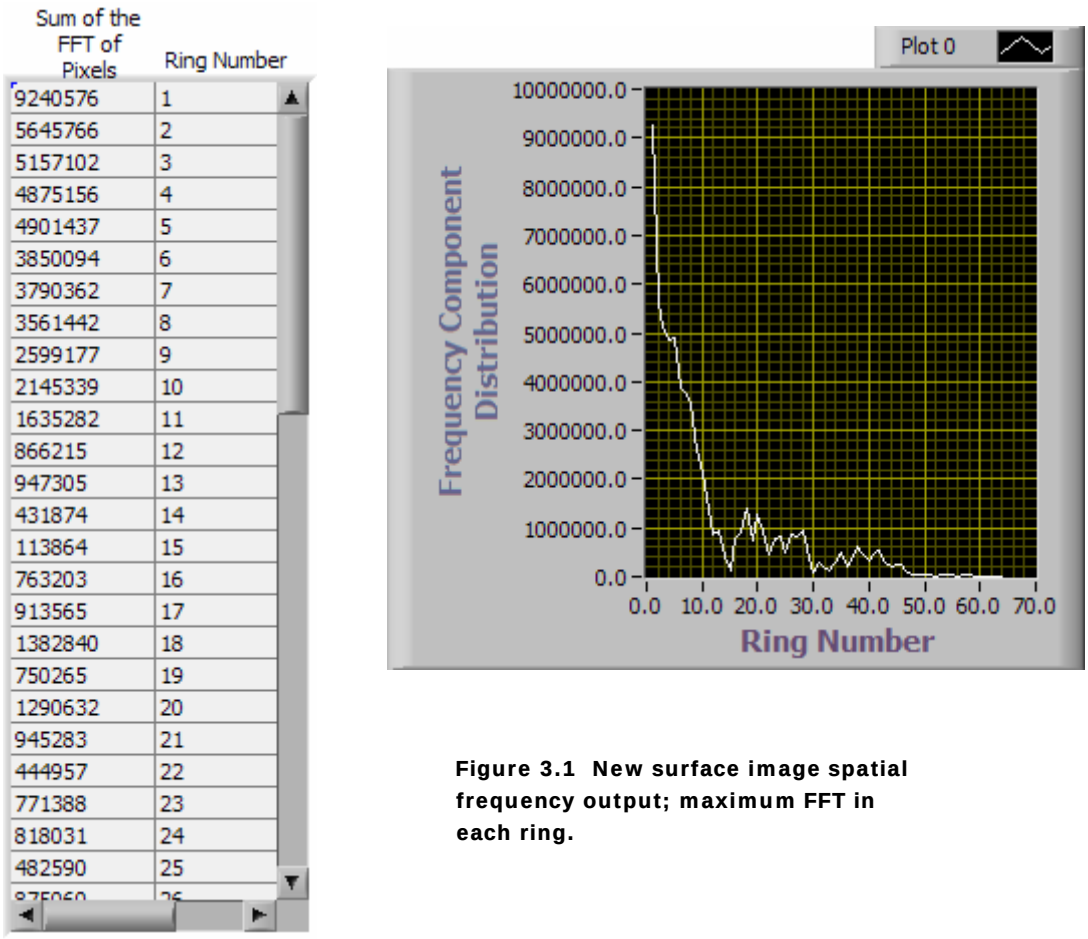

Sum of the FFT of Pixels	Ring Number
9240576	1
5645766	2
5157102	3
4875156	4
4901437	5
3850094	6
3790362	7
3561442	8
2599177	9
2145339	10
1635282	11
866215	12
947305	13
431874	14
113864	15
763203	16
913565	17
1382840	18
750265	19
1290632	20
945283	21
444957	22
771388	23
818031	24
482590	25

Figure 3.1 New surface image spatial frequency output; maximum FFT in each ring.

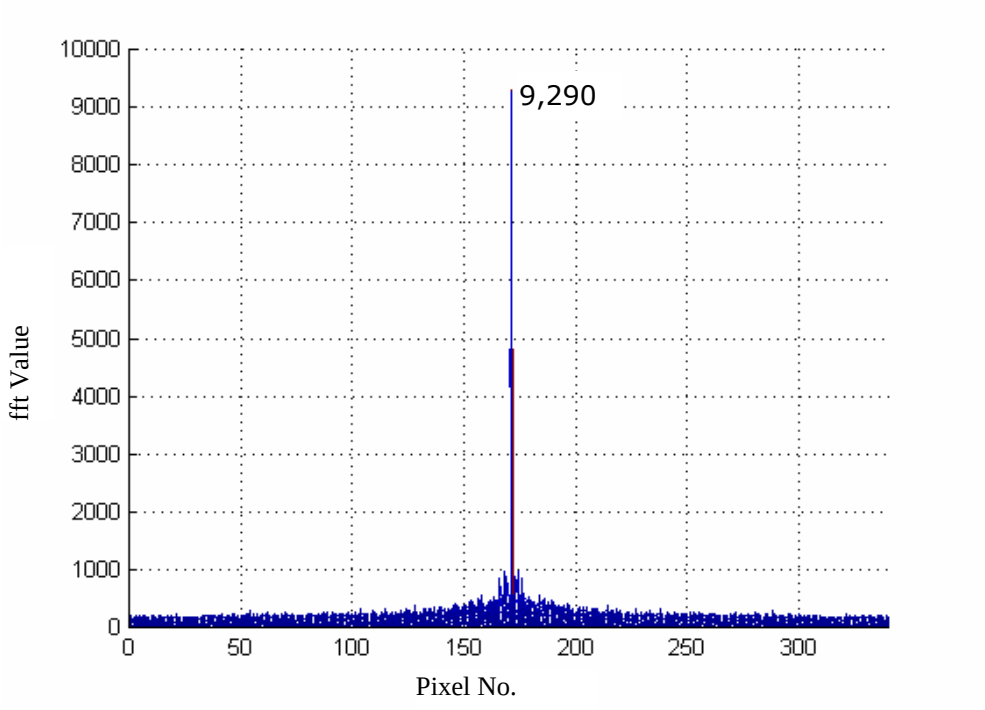

Figure 3.2 Previously published surface image spatial frequency output (Gransberg et al. 2002).

3.2 Trial software on sample phographs

To ensure that the procedure that worked in the US was directly translatable to New Zealand, Dr Gransberg travelled to Christchurch to participate in this step of the research methodology. The concern was that differences between US and New Zealand chipseal practices might affect the quality of the image processing output. Concerns were:

- the use of aggregate that had large variations in colour such as on the West Coast of New Zealand,
- the use of multiple grades of aggregate in New Zealand, rare in the US,
- the use in New Zealand of cutbacks, which are banned in the US.

A small number of sample chipseal digital images were taken of actual New Zealand seals and processed to verify that the image processing worked properly. The corresponding texture of the seals was also measured with the sand circle test at the same location as the image. The sample included single and multiple seals as well as several taken on the West Coast where the aggregate was not uniformly coloured. The test was very successful and the results are in this report.

3.3 Final data collection protocol

Based on the outcome of the previous step, the following protocol is to be applied when collecting digital image and sand circle data:

- Data must be collected and sorted by chip design type and chip grade. Initial regression models were able to achieve coefficient of determination (R^2) values in excess of 0.90 when the images were sorted in this fashion. Thus, separate regression models will need to be developed for each type and size of seal.
- Because of the low reproducibility of the sand circle test found in the literature (Patrick et al. 2000) and the inherent localised variation in chipseal surface texture itself (Christie 1954), an average derived from five sand circle tests taken approximately one metre apart (see Figure 3.3) should be used to form a composite texture measurement which will then be regressed against the average formed from the maximum FFT value for the processed images that correspond to the five locations.
- Multiple aggregate seals are problematic for the technology at this point in the research, because of the image-processing algorithm that depends on the edge detection feature in the software to quantify information content. Multiple aggregate seals have small particles nested inside larger particles and as a result contain a much larger number of edges than single seals. The software essentially 'interprets' a large number of edges as a satisfactory texture and a small number of edges as a flushed surface. Thus, the decision was made to focus the main effort on developing the technology for single seals first and then move to multiple aggregate seals in future research.

Figure 3.3 Sand circle testing protocol.

3.4 Final image processing protocol

The image processing protocol could be established once the variables discussed in Section 3.1 were determined. The image processing protocol is displayed in Figure 3.4, which illustrates both the process and the visual stages of a typical image as it is it processed along with the corresponding code that is associated with each step in the process. The image processing protocol furnishes the researchers with a direct means to quantify FFT output for up to 25 rings in each image. The literature shows that, when interpreting FFT output, the researcher must be careful to differentiate between actual luminance values and noise created by specular reflections. By dividing the image as previously discussed into rings by frequency band, the potential problem of controlling for noise is greatly diminished (Stemprok et al. 2000). Thus, this output data permits the researcher to search for FFT values in each ring to find which ring or set of rings give the best regression coefficients of determination and hence the strongest correlation with the physical texture measurements made using the sand circle test.

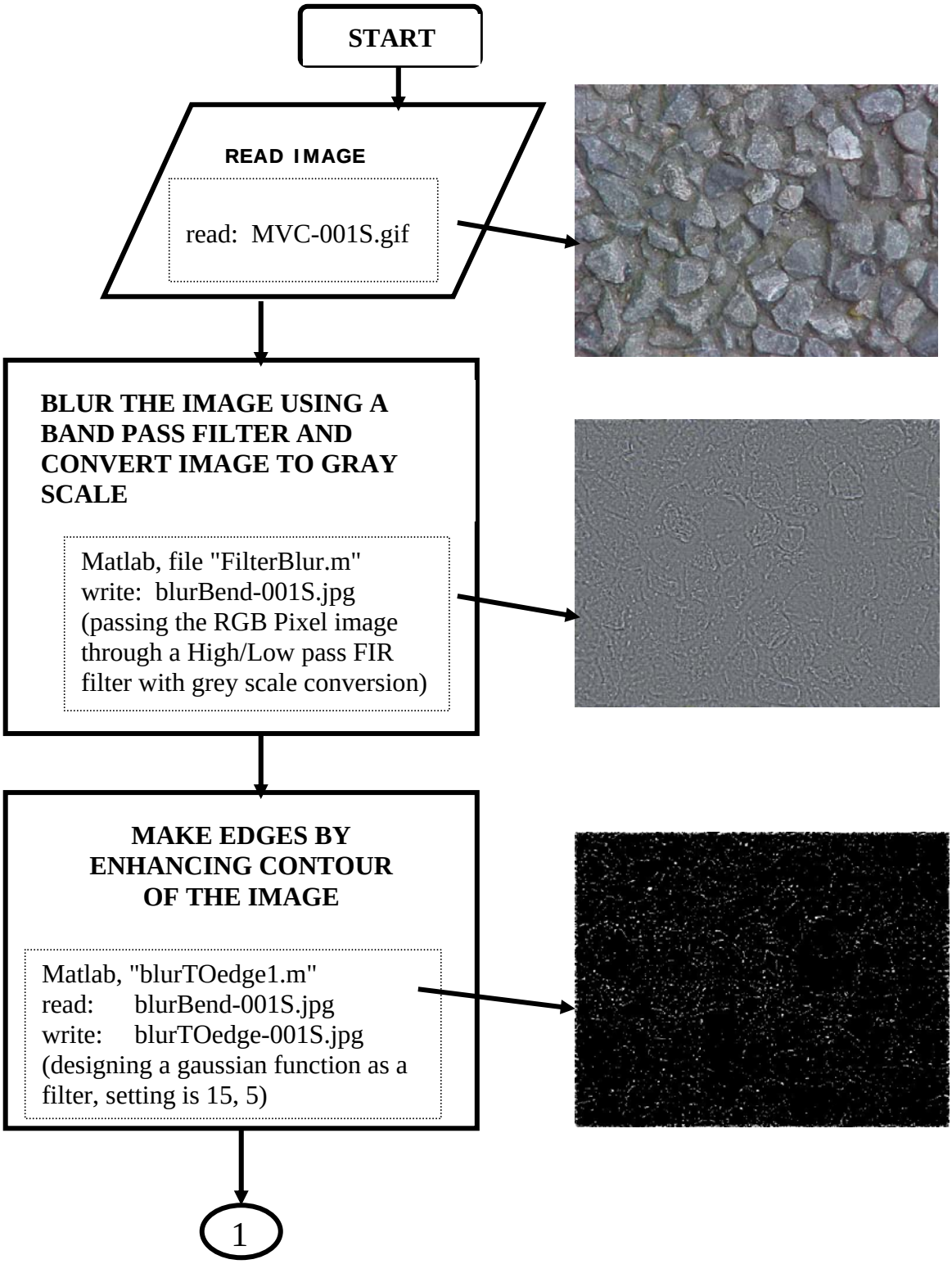

Figure 3.4: Image processing protocol (continued on next page).

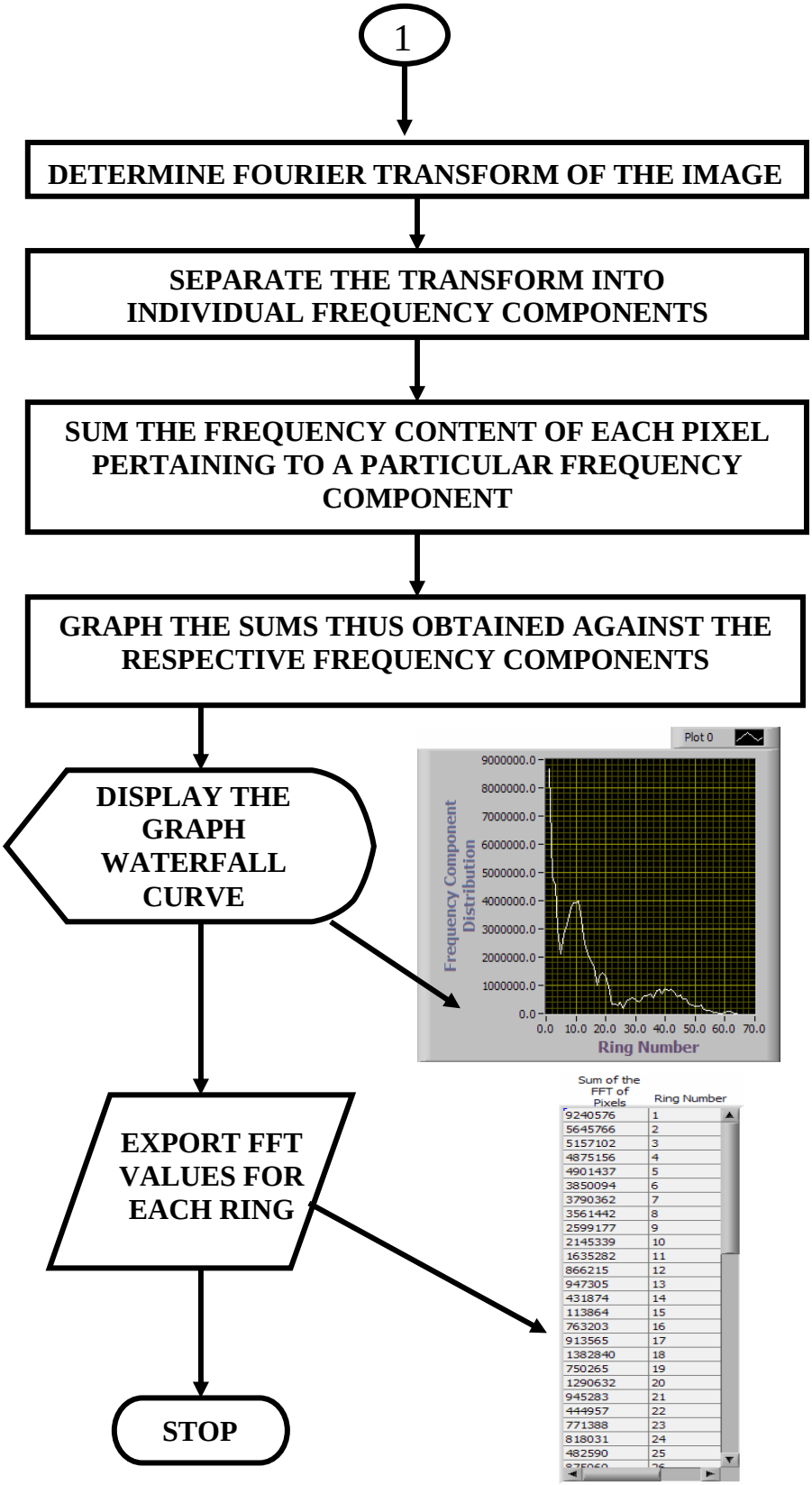

Figure 3.4 (continued) Image processing protocol.

4. Preliminary results

4.1 Results from Oklahoma trials

A series of limited experiments was run using the imaging processing software and protocol on digital images collected on Oklahoma chipseals in September 2004. The image processing output was correlated with qualitative ratings of chipseal texture to ensure that the new software and hardware could replicate the process published in Gransberg et al. (2002). The trials were successful and the researchers concluded that the experimental design was adequate to move to the next stage of the research.

Table 4.1 Oklahoma qualitative image/condition correlation in ring 10.

Condition #	Qualitative condition rating	FFT
1	Heavily flushed	4,417,352
2	Flushed and crackfillled	4,226,695
3	Flushed	5,454,247
4	Severe aggregate loss	3,109,902
5	Moderate aggregate loss	2,578,849
6	Slightly flushed	803,459
7	Minor aggregate loss	762,975
8	Medium texture	1,101,687
9	Medium texture	996,307
10	Good texture, good-looking seal	933,013
11	Good texture, best-looking seal	733,891

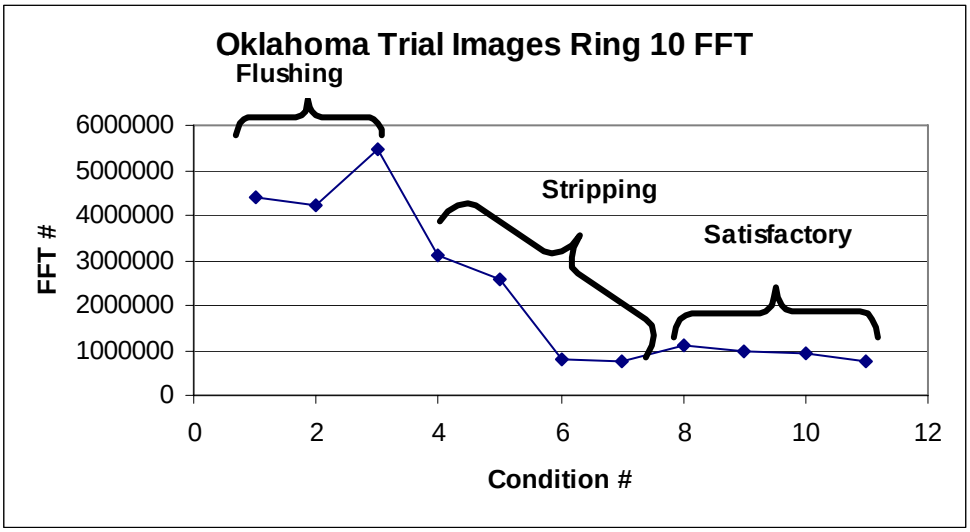

Figure 4.1 Oklahoma qualitative image/condition correlation in ring 10.

Table 4.1 and Figure 4.1 illustrate the outcome of these limited trials. With the exception of image condition number 6, the FFT number computed using the ring 10 output from each of the eleven images exhibit the behaviour that was predicted by the research reported in the journal article. The images of flushed chipseals seem to have the highest FFT numbers. The satisfactory textures show the lowest FFT numbers, and the seals that are experiencing a loss of aggregate fall somewhere in the middle. Even image 6 can be logically explained. It was qualitatively rated as 'slightly flushed.' Thus, the amount of binder that is exposed would be greater than the amount exposed in a satisfactory texture but less than the amount that would be exposed in a fully flushed surface. Mathematically, this appears to be in approximately the same range as those images where stripping is evident and as a result, there would be patches of exposed binder and other patches of satisfactorily imbedded aggregate. Therefore, it can be confidently concluded that the experimental design is yielding results that are consistent with those predicted in the literature.

One significant, though completely inconsequential, difference exists. The literature states that a satisfactory texture would yield a high FFT when compared to a flushed texture. In this experiment, that relationship is exactly reversed. This reversal is caused by the use of a more robust and sensitive version of the commercial software and the graphing of the inverse of what was graphed in the literature. Therefore, the relationship has not changed. Only the directional magnitudes have been reversed. As the purpose of this research is to differentiate between chipseal textures, it does not matter which surface condition has the higher or lower FFT magnitude. What matters is that a consistent mathematical differential exists that can be measured and correlated against the physical measurement of texture.

4.2 Results from New Zealand trials

Another series of limited experiments was run on digital images collected on New Zealand chipseals in October 2004. The output from the image processing in New Zealand was then correlated with the sand circle texture measurements taken at the same time and in the same locations as the images. Both linear and polynomial regression models were developed and the classic statistical measurement of correlation, the coefficient of determination (the R^2 value), was computed.

4.2.1 Proof of concept

Figures 4.2, 4.3, and 4.4 illustrate the image processing output derived from the digital images collected in New Zealand alongside the corresponding image. In the region of ring 10 a pronounced difference in FFT values occurs. This graphically illustrates the importance of applying this type of analysis to the problem of chipseal texture measurement with a digital camera. Each of the 25 rings exhibits somewhat different behaviour and the research team will exploit this new knowledge to enhance the ultimate accuracy of the measurement technique.

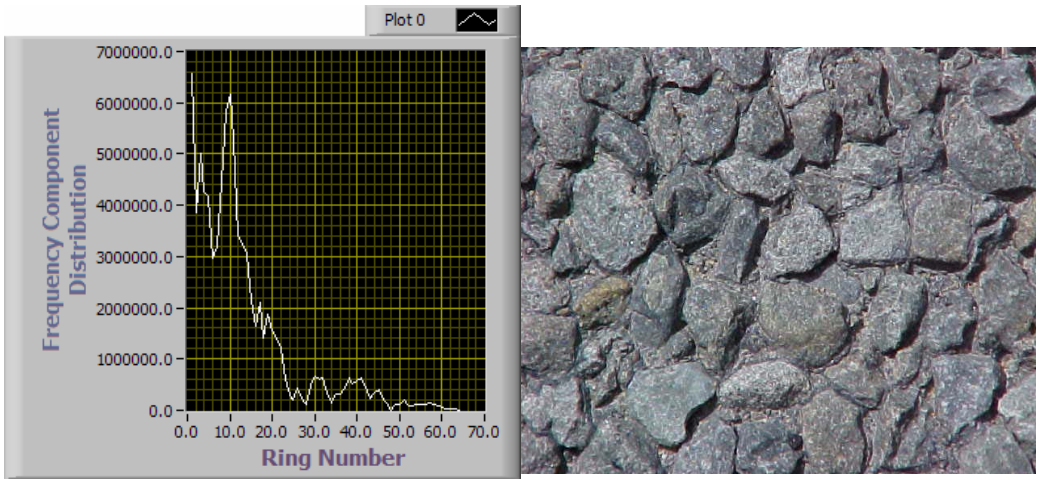

Figure 4.2 Satisfactory texture; grade 3 single chip; 175 mm sand circle.

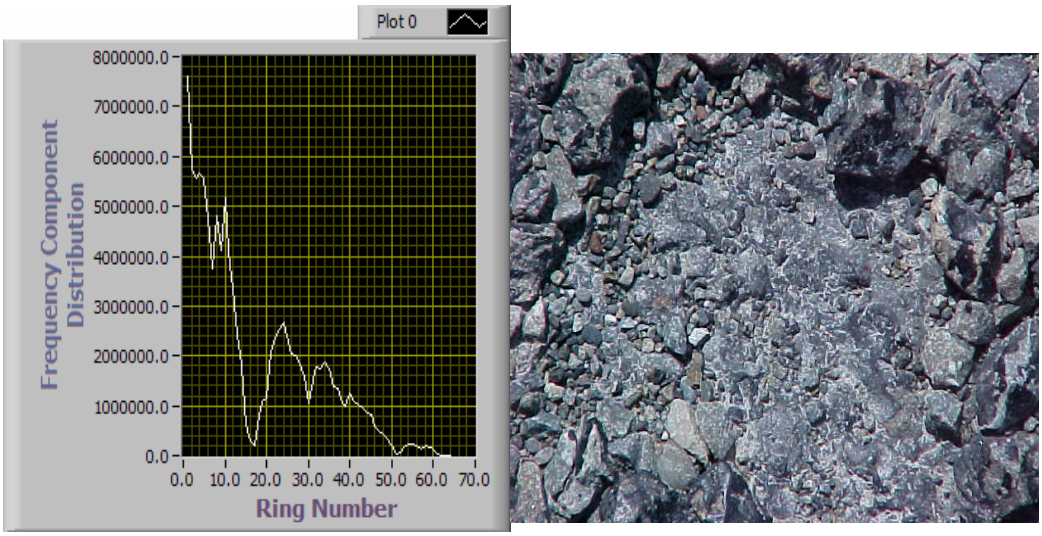

Figure 4.3 Major aggregate loss; grade 2 and grade 5 multiple chip; no sand circle measurement.

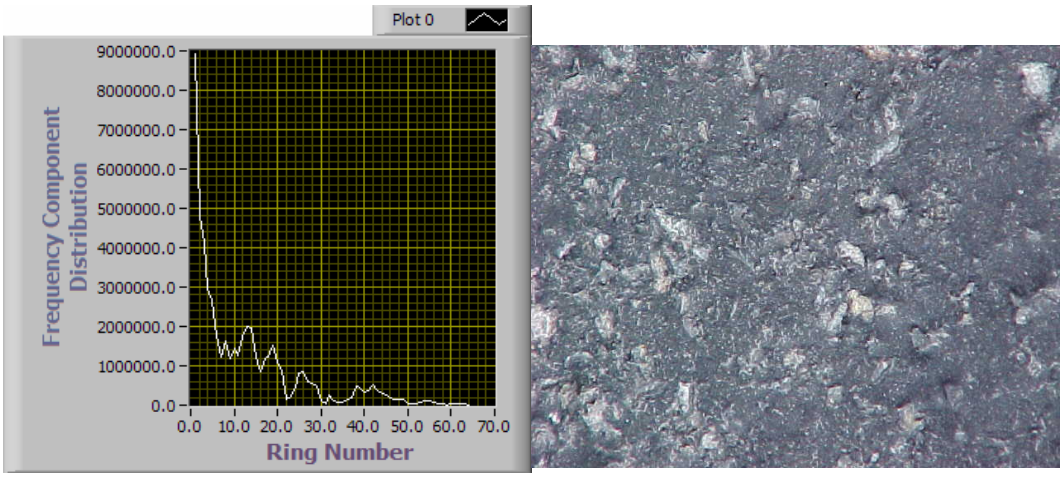

Figure 4.4 Very heavy flushing; grade 3 single chip; 300 mm sand circle.

The ring 10 phenomenon in the previous discussion needs further explanation. Figures 4.2 and 4.4 are of the same size chip and were taken using the same camera at the same focal length. One can easily observe that the FFT value for satisfactory chipseal texture (Figure 4.2) is around 6.1 million whereas when the surface becomes heavily flushed that it drops to around 1.2 million. One can see that the sand circle measurement nearly doubles between the two images. It is also interesting to note in Figure 4.3 (the image portraying aggregate loss) that the ring 10 FFT is something less that 5.0 million. While this is a different chipseal design, thus making the comparison indirect, the concept that the FFT and hence the information content should reduce as the amount of visible aggregate – binder edge boundaries decreases is validated.

4.2.2 Proof of principle

Table 4.2 contains the information on the image/sand circle tests that were taken in New Zealand. A cross-section of typical New Zealand chipseals has been included in the population. Additionally, typical chipseal distresses were also included.

Table 4.2 New Zealand trial image sample population.

Image Sequence	Design	Texture	Sand Circle (mm)
#2	2-coat grade 2 & grade 4	Satisfactory	145 mm
#3	West Coast grade 5 variegated colour chip	Satisfactory	185 mm
#5	2-coat grade 2 & grade 5	Minor aggregate loss	150 mm
#6	2-coat grade 2 & grade 5	Major aggregate loss	120 mm
#7	Single grade 3	Very heavy flushing	300 mm
#8	Single grade 3	Heavy flushing	285 mm
#9	Single grade 3	Satisfactory	175 mm
#10	2-coat grade 3 & grade 5 greywacke	Overchipped	160 mm
#11	Single grade 2	Slight flushing	180 mm
#12	Single grade 2	Satisfactory	155 mm

Initially the hope was that sorting images out by design type would not be needed as the work in Texas was not diminished by the inclusion of images that contained not only two different chip gradations, but also a combination of precoated and non-precoated chips in the sample. However, the correlations made in the Texas study were between a qualitative condition rating and the quantitative output of the image analysis. When the same approach was applied to correlating two quantitative measures for the entire sample population (i.e the sand circle and the FFT value), the effort was less successful. Figure 4.5 is a graph that shows the highest correlation. This effort was only able to achieve a coefficient of determination (R^2) of 0.4237, which means that the FFT accounts for only 42 % of the variation in the sand circle measurement. This is unacceptable, although interestingly, this would put the use of the camera to measure chipseal in the same rough range of variability as the sand circle test.

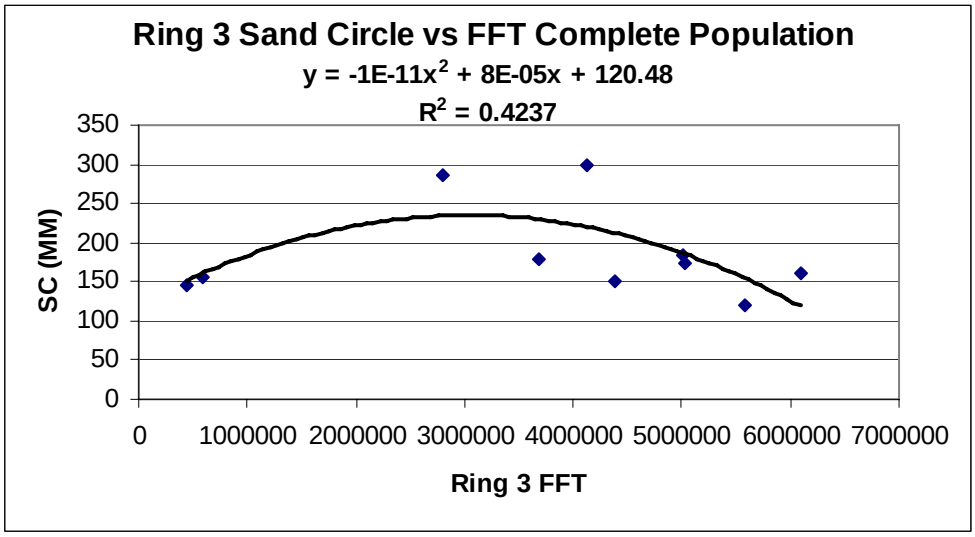

Figure 4.5 Attempt to correlate sand circle measurement and FFT value for complete population.

An attempt was then made to explain the seeming failure of the regression analysis. The explanation must lie in the visual variety that was presented in the sample population. As the FFT value is a function of the number of edge boundaries present in the image, the team then tried sorting the double chipseals from the single chipseals. The justification was that the double chipseal, which incidentally is not used in the US, creates an image with a much higher number of edge boundaries and may need to be correlated as a separate group. This produced the correlation shown in Figure 4.6. This increased the coefficient of determination (R^2) to 0.6316, thus improving the statistical correlation.

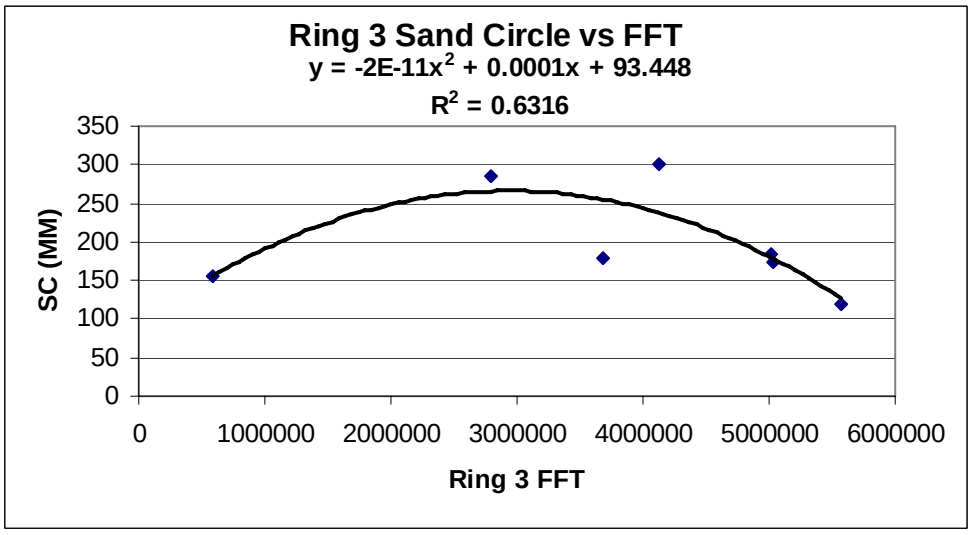

Figure 4.6 Attempt to correlate sand circle measurement and FFT value for single chipseals only.

The population of single chipseals included one seal that used grade 2 chips that are larger than the grade 3 chips used in the remainder of the population. This data point was removed and the results are shown in Figure 4.7. With a coefficient of determination (R^2) of 0.9387, this furnished a satisfactory result and demonstrates the potential for a strong improvement in variability over the sand circle test.

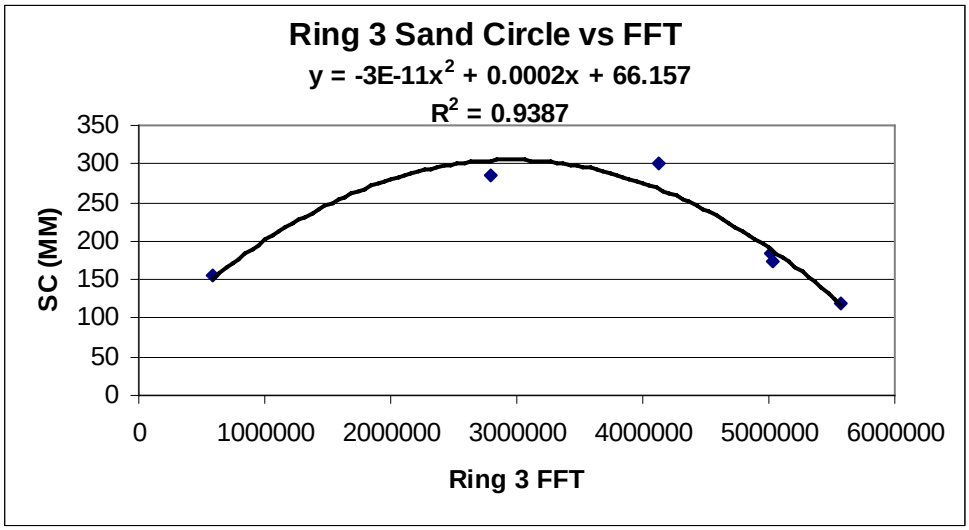

Figure 4.7 Correlation of sand circle measurement and FFT value for grade 3 single coat chipseals only.

5. Final grade 3 single-size chipseal results

Based on the issues found in the preliminary trials, the decision was made to focus the final effort on establishing the texture/FFT relationship for grade 3 single-size chipseals before moving on to other seal design types later, as time and resources permitted.

A database of image and sand circle test observations was developed. After filtering out those images that had suffered some form of data corruption or were not made according to the final protocol, the team was left with a total of 35 images of grade 3 single-size chipseal surfaces and their corresponding sand circle measurements. These were ultimately grouped into seven sets of photos from the same locations which could be averaged together in accordance with the data collection protocol discussed in Section 3.3. This procedure produced FFT values that could then be regressed against both sand circle measurements and ultimately calculated texture depths based on the sand circle measurements.

The researchers returned to the field to collect additional images of flushed chipseal surfaces as the attempt to find correlation with randomly selected surfaces had failed. Two groups of flushed images (sand circle > 250 mm) were added to the base population. Two groups of satisfactory texture (sand circle < 180 mm) images, for some unknown reason, had a decidedly blue-coloured cast (causing the researchers to question the validity of the FFT values). These were removed to give a better balance to the base population. Nevertheless, the final population was somewhat weighted toward the satisfactory end of the texture spectrum.

The potential size of the mathematical analysis required to isolate the portions of the processed digital image output is huge. As previously discussed, most of the change in FFT value occurs in the first 25 rings of the processed image. Thus, the analyst needed to break those rings out in logical combinations to determine which combination created the strongest correlation with the physical measurements. To do a factorial analysis of combinations is prohibitive as there are theoretically 1.55×10^{25} possible combinations of 25 rings. Thus, the analysis was constrained to a reasonable number of combinations as follows:

- each ring individually; rings 1 to 25,
- the sum of rings 1 to 5; 6 to 10; 11 to 15; 16 to 20; and 21 to 25,
- the sum of rings 1 to 10; 6 to 15; 10 to 20; and 15 to 25,
- the sum of rings 1 to 15; 6 to 20; and 11 to 25,
- the sum of rings 1 to 20 and 6 to 25,
- the sum of rings 1 to 25.

5.1 Individual ring results

The results of this analysis were inconclusive. Nevertheless, they were very instructive and assisted in furnishing a good synopsis of the behaviour of FFT values within the processed image itself. Three different possible FFT values were evaluated against their corresponding sand circle measurements for all 25 rings (a total of 75 different comparisons).

- The discrete FFT value that was observed in the given ring for each group was regressed against the sand circle diameter, e.g. FFT (ring 6) v sand circle.
- The cumulative FFT at the given ring was regressed against the sand circle diameter, e.g. 3FFT (rings 1 to 6) v sand circle.
- The normalised FFT at the given ring was regressed against the sand circle diameter, e.g. [3FFT (rings 1 to 6)/ FFT (ring 10)] v sand circle.

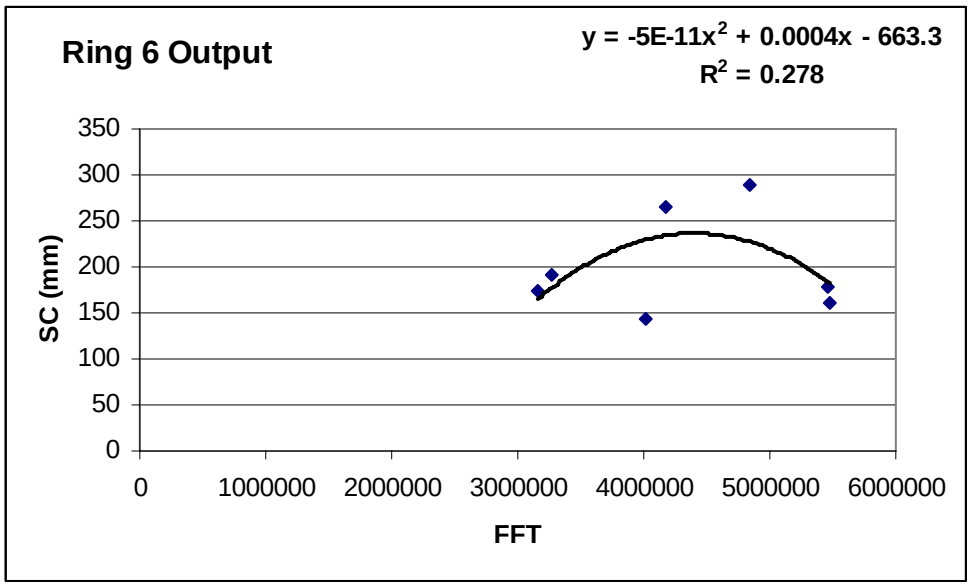

Figure 5.1 Typical regression output for individual ring analysis.

Figure 5.1 shows the graphical output that was developed for ring 6 of the data population and is typical of the output for this piece of the mathematical analysis. The highest coefficient of determination (R^2) that was achieved was 0.278 which corresponds to a 2nd order polynomial curve generated to fit the points in ring 6. Linear equations had the lowest R^2 values and increasing the order of the polynomial equation generally increased the R^2 value. While this would seem to be an improvement, in reality it was not because of the complexity of the curve generated by 3rd and 4th order polynomial equations. The data were also tested for fit using exponential, power and logarithmic equations to no avail. The best R^2 values were obtained from the polynomial equations and the conclusion was that the relationship can be best characterised by this mathematical expression.

An analysis of the R^2 values indicated that the best results were seen in rings 6 to 10. This helped the researchers establish the groupings in sets of five as discussed in Section 5.2. It also showed the potential for achieving reasonable results. The change in R^2 values between individual rings of the same image group was extremely volatile and there were no apparent trends other than the one regarding the rings that had the highest R^2 values.

5.2 Groups of five rings results

A similar analysis was run on FFT values grouped by sets of five rings. For this analysis, the images were divided into their individual groups and the average FFT value in each of the first 25 rings was taken for each group using the following equation:

$$\text{Average FFT (ring 6 to 10)} = 3\frac{\text{FFT (rings 6 to 10)}}{5} \qquad \text{Equation 5.1}$$

That was then taken as the value to be used in the regression analysis against the sand circle measurement. Table 5.1 contains the results of that analysis. Again it can be seen that the best results were received from polynomial equations and increasing the order of the polynomial equations increased the coefficient of determination. However, outcomes were restricted to polynomials of the second order because of the complexity of the curves generated by higher order polynomials.

Table 5.1 Five ring group regression analysis results.

Ring Group	Linear Equation	R^2 Value	Polynomial Equation	R^2 Value
1 to 5	y = 3492.7x + 5E+06	0.0640	y = -55.127x^2 + 27662x + 2E+06	0.0818
6 to 10*	y = 5.0606E-5x + 30.54	0.2060*	y = 2.63458E − 10x^2 − 0.00163x + 2653.3	0.7513*
11 to 15	y = −2541x + 3E+06	0.0976	y = 77.358x^2 − 36457x + 6E+06	0.1983
16 to 20	y = −1150.9x + 1E+06	0.0594	y = 92.594x^2 − 41747x + 6E+06	0.4880
21 to 25	y = −1981.1x + 1E+06	0.2514	y = 58.245x^2 − 27517x + 4E+06	0.4934

*Equations shown in table have been manually regressed to get more accurate coefficients.

Table 5.1 shows that the strongest correlations were found in the ring 6 to 10 group. This fits with the results of the previous analysis as well as the visual inspection of the waterfall graphs generated from the raw digital image output that showed the major change in FFT between satisfactory texture images and flushed images occurred in the ring 6 to 15 range.

5.3 Other groups of rings results

The process described in the previous section was repeated with other groups of rings in increasing sizes of sets listed in the introduction to Chapter 5. Only the significant results will be reported at this point.

Analysis of the remaining groups of rings yielded two significant outputs.

First, the reader should remember that these groups were using increasingly larger amounts of the available information output, and thus, were becoming increasingly representative of the total information content of the normalised image group being regressed with the physical measurement. The first significant result was from the group that utilised the average of the sum of rings 1 to 20. Though the statistical correlation was low, it was significantly higher than virtually all the other attempts with various ring groups. Figure 5.2 shows that an R^2 value of 0.59 was obtained when the data were regressed against the sand circle diameter.

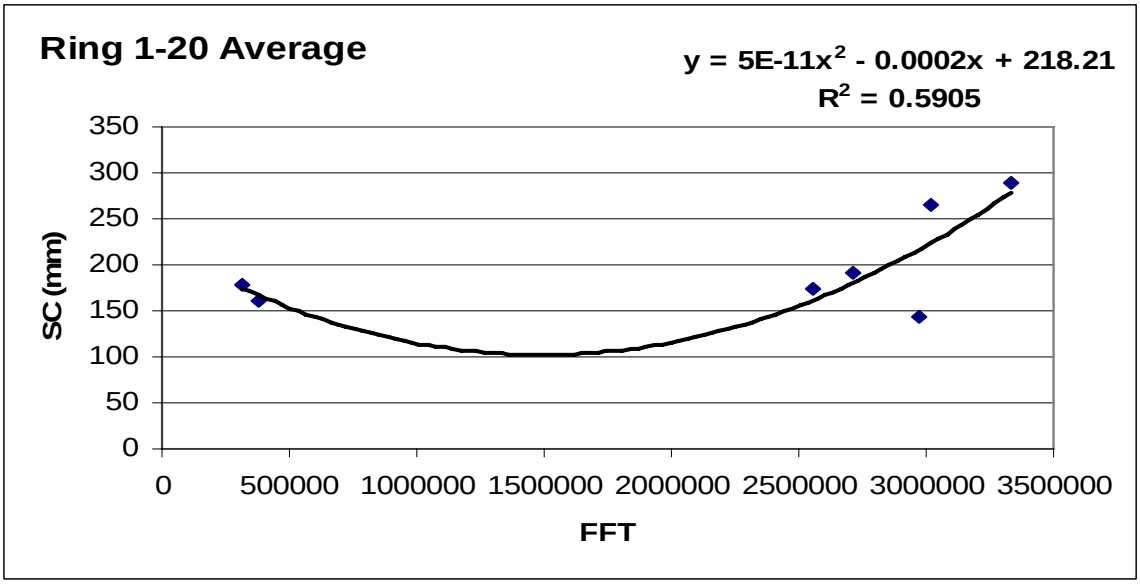

Figure 5.2 Rings 1 through 20 average regressed against the sand circle measurement.

The second and most significant result came when the sand circle measurement was converted to average texture depth using Equation 2.1 and the resulting texture depths were regressed against the average of the sum of the FFT values in rings 1 to 25. A strong correlation indicated by an R^2 value of 0.80 was obtained in this case. As this contains the majority of the information that is contained in the image group, this conclusively proves that texture can generate a mathematically measurable relationship in a digital image group.

Figure 5.3 is technically correct for this particular project where the texture component is the independent variable in the regression sequence (i.e. the parameter that was actually measured in the experiment) and the FFT value is the dependent variable (i.e. the parameter that is predicted from the independent variable). To extend this theoretical finding into practical application the situation would be reversed, and the measurement would be derived from the digital imagery and used to predict the average texture depth of the surface that had been imaged. Thus, the regression was reversed and the FFT values were moved to the X-axis and the texture was moved to the Y-axis. Figure 5.4 shows the results of this exercise and the correlation is understandably reduced by the reversal in axes.

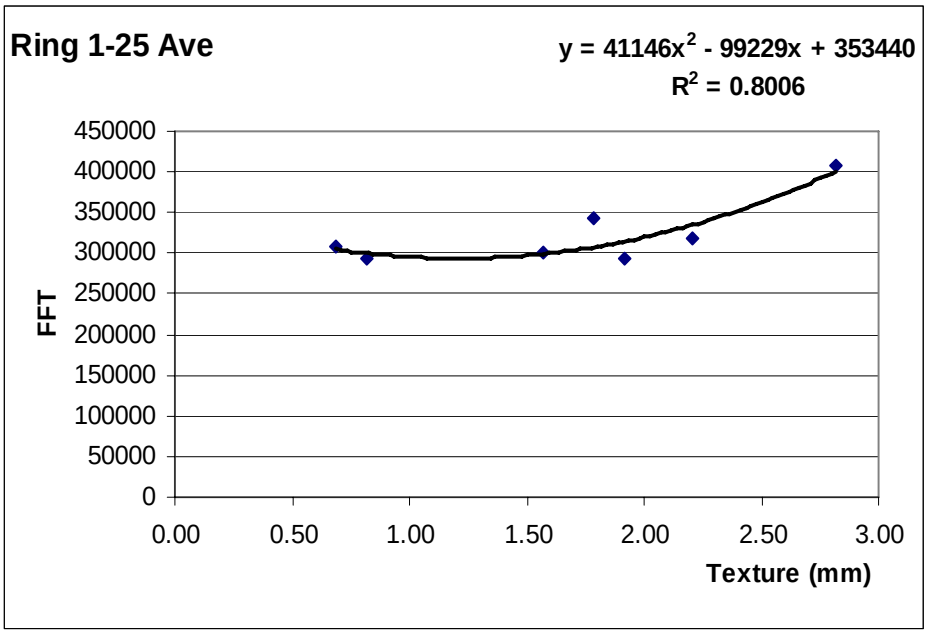

Figure 5.3 Rings 1 to 25 average FFT regressed against the calculated average texture depth value.

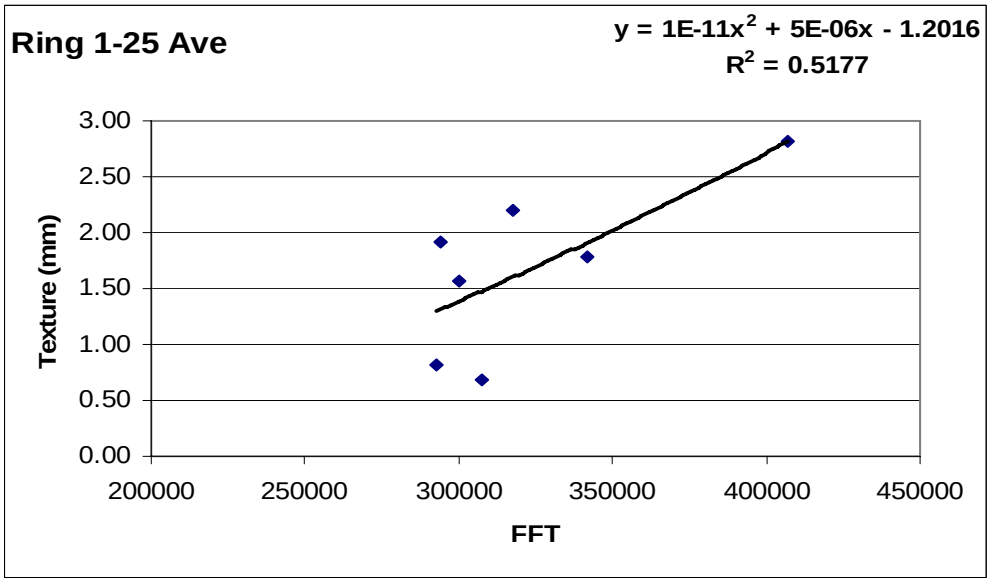

Figure 5.4 Calculated average texture depth value regressed against rings 1 to 25 average FFT.

This section must be concluded with a word of caution regarding the equations generated by the linear regression function in Microsoft Excel®. The relative order of magnitudes difference between the FFT values that in the analyses were in the 10^5 to 10^6 range versus the sand circle measurements in 10^2 millimetres, or average texture depth in the 0 to 3 millimetre range, makes the rounding convention for those coefficients expressed in scientific notation used in Microsoft Excel® unsatisfactory for replicating the data analyses. All the significant results were checked using a manual regression function in Microsoft Excel® called 'LINEST.' When this was used, the rounding convention was found to have rounded to the nearest power of ten, and when the equations were rewritten used

ten significant digits, the input-output relationship was found to be accurate. For example, in Table 5.1, ring group 6 to 10 originally showed the first term in the polynomial to be " $-3E-11x^2$" after applying the Microsoft Excel® 'Add Trendline' wizard. When regressed manually, the term is actually "$-2.63458\ E-10x^2$."

When typical values for 'x' were fed into the original conventionally rounded term, impossible values for 'y' were returned because of the large difference in orders of magnitude between 'x' and 'y'. Checking the output values for the equation using the coefficient derived from the manual regression solved this problem and returned reasonable 'y' values. Therefore, the reader is cautioned against attempting to directly 'check' the validity of the equations shown on some of the graphs that utilise scientific notation because of the error that is introduced by the rounding conducted by the software.

6. Conclusions

The following is a list of conclusions that were reached in this research project.

1. The literature supports the need for an accurate, reproducible method to measure chipseal surface texture. Texture is directly related to skid resistance. This measurement is also important to the design of reseals to achieve the proper aggregate gradation and bitumen amount that not only achieves the desired pavement preservation objectives but also improves the physical characteristics of the newly sealed surface. Developing a method that allows road authorities and their contractors to enhance the safety, reproducibility, and rate of texture measurements will be beneficial.

2. The literature also supports the use of digital imaging and image processing using the FFT as a means to quantify physical characteristics contained in an image. The Texas study proved that this approach could be used to correlate surface condition and information content. Quantifying information content as the primary measurement makes sense in that, as a chipseal surface deteriorates through either flushing or aggregate loss, the number of edge boundaries between the chips and the binder decrease, which intuitively decreases the amount of information in the image. Correlating information content using the FFT value with a physical texture measurement is a logical step in developing this technology for use in public roadway pavement management information systems.

3. The results of the limited trials in Oklahoma and New Zealand clearly demonstrated that merging digital image processing and physical texture measurements is possible and the potential to replace the sand circle test with a digital camera is high. The researchers were able to validate both the concept and the principle through the initial set of experiments. These allowed the team to standardise the experimental setup and calibrate the software and hardware necessary to achieve a strong correlation using linear regression analysis with a sorted sample population.

4. Exploiting the edge boundary phenomenon caused difficulties as well as successes. Most notable was the inability of the current algorithm to deal with multiple-size chipseals. The research team had to remove samples from the population that were not of the same size and design in order to achieve strong statistical correlation between the images and the sand circle measurements. Thus, separate models will be required for each standard chipseal design because each design creates a different average number of edge boundaries between the chips and the binder. As a result, the conclusions reached in the study are only directly applicable to the grade 3 chipseals that were in the homogenous sample population. Nevertheless, most of the conclusions can be generalised for other chipseal designs.

5. The current methodology may not be useful in developing a model for chipseals that are losing aggregate. The major issue with aggregate loss is not in the imaging technology but rather in the sand circle test where it becomes extremely difficult to

accurately apply the test if the 'hole' in which the aggregate is missing is relatively large. This is because the standard volume of sand can literally fail to fill the 'hole' and as a result no accurate area of sand can be measured. An alternative method of accurately correlating the image output with the size of the area of lost aggregate would be needed, but this is beyond the scope of this research.

6. The major goal of the research was to prove that a relationship exists between chipseal texture (as measured by the sand circle test) and digital image output (as measured by a function of the FFT of the digital image). The correlations were sought in both directions, i.e. texture versus FFT and FFT versus texture. Additionally, the texture component was looked at in two ways: using the sand circle diameter, and using the computed texture depth. A number of strong correlations between image output and physical measurements were found:

    a. The data was regressed using linear, polynomial, power, exponential, and logarithmic curves. In all tested cases, the best-fit curve was a second order polynomial equation. Therefore, it is concluded that the relationship between texture and FFT is a polynomial expression.

    b. When the calculated texture depth was taken as the independent variable and a linear regression equation of the best-fit curve was developed using the average of the sums of FFT values in rings 1 to 25, a coefficient of determination (R^2) of 0.80 was derived indicating that the texture depth explains approximately 80% of the variations observed in the FFT component to the regression analysis. The equation is a second order polynomial: $y = 41146x^2 - 99229x + 353440$. This conclusively confirms the notion that physical texture can generate a measurable function in a digital image.

    c. When the process is reversed (i.e. texture is the dependent variable and FFT is the independent variable) the correlation is reduced with the R^2 value dropping to 0.52. This is understandable in that this analysis is 'artificial' based on the experimental methodology.

    d. When the actual sand circle diameter measurement is regressed against various combinations of ring FFT values, the best correlation was found with the average of the sums of FFT values in rings 1 to 20. A coefficient of determination (R^2) of 0.51 was derived indicating that the sand circle diameter explains approximately 51% of the variations observed in the FFT component to the regression analysis. The equation is a second order polynomial: $y = -175.78x^2 + 88477x - 8E+06$.

    e. When the axes are reversed the correlation increases with an R^2 value of 0.59.

    f. Using higher order polynomials for the regression equation tends to increase the R^2 values for most situations. However, these are not recommended as they generate complex curves that will be difficult to use in eventual field applications. A linear relationship would be preferred to simplify moving this

technology from research to field application. The linear regression of the relationship described in subparagraph 6b above yields an R^2 value of 0.52, not much better than the 0.40 reproducibility of the sand circle test.

g. Other combinations of ring FFT values may exist that yield stronger correlation to either texture depth or sand circle diameter that were not tested in this project. These will need to explored in future research.

7. The technology's ability to accurately measure and correlate the difference between satisfactory texture and texture that is flushed is excellent. Thus, the chipseal failure condition that corresponds to a pavement surface condition which presents the greatest danger to the travelling public is covered by the proposed technology.

2. Bibliography

ARRB. 2001. Variation in surface texture with differing test methods. Unpublished report prepared for National Bituminous Surfacings Research Group by ARRB Transport Research: Melbourne, Australia.

Asphalt Institute. Undated. Asphalt surface treatments – construction techniques. *Educational Series No. 12 (ES-12).* Asphalt Institute: Lexington, Kentucky, USA.

Asphalt Institute. Undated. Asphalt surface treatments – specifications. *Educational Series No. 11 (ES-11)*. Asphalt Institute: Lexington, Kentucky, USA.

Asphalt Institute. 1997. A basic emulsion manual*. Manual Series No. 19.* 3rd ed. Asphalt Institute: Lexington, Kentucky, USA, and the Asphalt Emulsion Manufacturers Association: Annapolis, Maryland, USA.

ASTM. 2001. *E965-96. Standard test method for measuring pavement macrotexture depth using a volumetric technique*. ASTM: West Conshohocken, Pennsylvania, USA.

ASTM. 2003. *E2157-01 Standard test method for measuring pavement macrotexture properties using the Circular Track Meter*. ASTM: West Conshohocken, Pennsylvania, USA.

Austroads. 2000. *Austroads provisional sprayed seal design method*. Austroads: Sydney, Australia.

Austroads. 2004. *Sprayed sealing guide*. Austroads: Sydney, Australia.

Benson, F.J., Galloway, B.M. 1953. Retention of cover stone by asphalt surface treatments. *Bulletin 133, Texas Engineering Experiment Station.* Texas A&M University System: College Station, Texas, USA.

Bose, T. 2004. *Digital signal and image processing.* John Wiley & Sons: New York, New York, USA.

Bracewell, R. 1965. *Fourier transform and its applications.* McGraw-Hill: New York, New York, USA.

Brigham, E.O. 1974. *Fast Fourier transform.* Prentice Hall: Englewood Cliffs, New Jersey, USA.

Brigham, E.O. 1998. *The fast Fourier transform and applications*. Prentice Hall: Englewood Cliffs, New Jersey, USA.

Christie, A.W. 1954. Reflection characteristics of pavement surfaces. *Highway Research Board Bulletin 89:* 21-37.

Croakin, C., Tobias, P. 2005. *NIST engineering statistics handbook.* National Institute of Standards and Testing. Accessed May 23, 2005 from: *http://www.itl.nist.gov/div898/handbook/pmd/section1/pmd141.htm*

Cuvalci, O., Gransberg, D.D., Green, B., Nuhrat, C. 1999. Visibility measurement technique using photometric images. *1999 Annual ASEE Conference Proceedings, Session 3659.* Charlotte, North Carolina, USA. *http://www.asee.org*

Culvalci, O., Tanju, B.T., Gransberg, D.D., Green, B.L., Gransberg, N.J. 1998. Design and analysis of luminance, illuminance measuring system using video images. *Proceedings, Third Biennial World Conference on Integrated Design and Process Technology 5:* 66-74. Society for Design and Process Science: Berlin, Germany.

Duffieux, P.M. 1983. *The Fourier transform and its applications to optics. 2nd ed.* John Wiley & Sons, New York, New York, USA.

Ellis, K.L. 1976. Measurement of directional reflectance of pavement surfaces and development of computer techniques for calculating luminance. *Journal of the IES 5(2):* 118-126.

Goodman, J.W. 1968. *Introduction to Fourier optics.* McGraw-Hill: New York, New York, USA.

Goodman, S., Hassan, Y., Abd El Halim, A.O. 2004. The road to cost effective urban pavement friction measurement. *SURF 2004 5th Symposium on Pavement Surface Characteristics on CD.* Toronto, Canada.

Gransberg, D.D., Senadheera, S., Karaca, I. 1998. Analysis of statewide seal coat constructability review. *Texas Department of Transportation Research Report TX-98/0-1787-1R.* Texas Tech University: Lubbock, Texas, USA.

Gransberg, D.D., Karaca, I., Burkett, W.R. 2002. Quantifying seal coat surface condition using digital image processing based on information theory. *International journal of pavement engineering 3(4):* 197-205.

Gransberg, D.D., James, D.B.M. 2005. Chips seal best practices. *National Cooperative Highway Research Program Synthesis 342:* 17-19. Transportation Research Board: National Academies, Washington, DC, USA.

Griffith, A., Hunt, E. 2000. Asphalt cement chip seals in Oregon. *Construction Report OR-RD-01-01,* Oregon Department of Transportation Research Unit, Salem, Oregon, USA.

Hanselman, D., Littlefield, B. 2001. *Mastering MATLAB 6, a comprehensive tutorial and reference.* Prentice Hall: New York, New York, USA.

Hanson, F.M. 1935. Bituminous surface treatment of rural highways. *Proceedings, New Zealand Society of Civil Engineers 21:* 89-179.

Hecht, E. 1975. *Schaum's outline of theory and problems of optics.* McGraw-Hill: New York, New York, USA.

Henry, J.J. 2000. *NCHRP synthesis of highway practice No. 291: Evaluation of pavement friction characteristics.* TRB, National Research Council: Washington, DC, USA.

Holmgreen, R.J., Epps, J.A., Hughes, C.H., Galloway, B.M. 1985. Field evaluation of the Texas seal coat design method. *Research Report 297-1F.* Texas Transportation Institute, Texas A&M University System: College Station, Texas, USA.

Ifeachor, E., Jervis, B. 2002. *Digital signal processing.* 2nd ed. Prentice Hall: New York, New York, USA.

MATLAB®. 1997. *The language of technical computing*. The MathWorks, Inc.: Natick, Massachusetts, USA.

MATLAB®. 2000. *Image processing toolbox.* The MathWorks, Inc.: Natick, Massachusetts, USA.

McLeod, N.W. 1960. A general method of design for seal coats and surface treatments. *Association of asphalt paving technologists 38.* St. Paul, Minnesota, USA.

McLeod, N.W. 1969. Basic principles for the design and construction of seal coats and surface treatments. *Association of asphalt paving technologists* 38. St Paul, Minnesota, USA.

McLeod, N.W. 1974. *Seal coat and surface treatment design and construction using asphalt emulsions*. Asphalt Emulsion Manufacturers Association: Washington, DC, USA.

Meyer-Arendt, J.R. 1972. *Introduction to classical and modern optics.* Prentice-Hall: Englewood Cliffs, New Jersey, USA.

Montana Department of Transportation. 2000. *Maintenance chip seal manual*. Montana Department of Transportation: Helena, Montana, USA.

Moulthrop, J. 2003. *Pavement preservation: Protecting the investment*. Presentation made at NEAUPG Annual Meeting, Wilkes-Barre, Pennsylvania, USA.

National Cooperative Highway Research Program. 1989. Evolution and benefits of preventative maintenance strategies. *Synthesis of highway practice No. 153.* National Cooperative Highway Research Program, Transportation Research Board: Washington, DC, USA.

Owen, M. 1999. Managing the risk in a new performance based environment*. Conference on Asphalt Pavements for Southern Africa*: Zimbabwe.

Patrick, J.E., Cenek, P.D., Owen, M. 2000. Comparison of methods to measure macrotexture. *Proceedings 1st International Conference World of Asphalt Pavements on CD*, Australian Asphalt Pavement Association: Sydney, Australia.

Stemprok, R., Green, B., Tang, Z. 2000. Calculated roadway lighting errors and measurement of visibility with CCD devices. *Proceedings of the Symposium of Commission Internationale De L'Eclaire, (CIE), Division 4 and 5 meeting*: Toronto, Canada.

Tang, Z. 1999. *Digital image processing and spatial frequency analysis of Texas roadway environments*. Master's Thesis, Texas Tech University: Lubbock, Texas, USA.

Texas Department of Transportation. 2003. *Seal coat and surface treatment manual.* Texas Department of Transportation: Austin, Texas, USA.

TNZ (Transit New Zealand). 1981. *TNZ T/3*. *Standard test procedure for measurement of texture by the sand circle method.* Transit New Zealand: Wellington, New Zealand.

TNZ (Transit New Zealand). 1993. *Bituminous sealing manual*. 2nd ed. Transit New Zealand: Wellington, New Zealand.

TNZ (Transit New Zealand). 2002. *TNZ P/17. Notes for the specification for bituminous reseals.* Transit New Zealand: Wellington, New Zealand.

Vercoe, J. 2002. Chip seal texture measurement by high speed laser. Unpublished research report. Fulton Hogan, Christchurch.

Williams, C.S., Becklund, O.A. 1989. *Introduction to the Optical Transfer Function.* John Wiley & Sons: New York, New York, USA.

Wilson, R.G. 1995. *Fourier series and optical transform techniques in contemporary optics, an introduction.* John Wiley & Sons, Inc.: New York, New York, USA.

Appendix: Data

This appendix contains the data that correspond to those figures that were used to justify this report's conclusions. It consists of two tables.

Table A1 contains the average ring FFT values for the 25 rings that were used in the analysis. It also shows the corresponding average sand circle measurement for each image group.

As discussed in the body of the report, image groups B and C were dropped from the analysis because the images were somehow corrupted and came out with a decidedly bluish cast to the photos. These were processed and returned seemingly reasonable FFT values, but the researchers had no confidence in their validity because of the bluish cast of the images.

Image group F was also eliminated. This group contained only two images that were not taken in the same location. Therefore, it did not conform with the image collection protocol. Interestingly, it was this group that gave the researchers the clue to go out and seek more images of flushed chipseals. Group F was taken during the preliminary trials in New Zealand and used to ensure that the software could differentiate between flushed and satisfactory chipseal surface texture. When this group was added to the initial set of images the correlation shown in Figure 4.7 was achieved.

Image groups I and J replaced group F giving the sample population two groups of flushed texture to go along with the five groups with varying degrees of satisfactory texture.

Table A2 contains the processed data for the sand circle measurements and average texture depth calculations paired with the corresponding FFT analysis output that were used to generate Figures 5.3 and 5.4. These are included as these two figures portray the significant conclusion of this study. Finally, it should also be noted for the record that image groups of typical New Zealand chipseals of other types were collected including grade 2 single seals and grade 2 and 5 double seals. However, the decision to focus on developing the relationship for grade 3 chipseals precluded their use.

Table A1 Image individual ring FFT values and sand circle measurements.

Image Group	A	D	E	G	H	I	J
SC_{av} * (mm)	191.0	173.0	142.5	179.0	161.3	289.0	265.0
Ring #	Average ring FFT value						
1	8,572,109	9,057,075	8,634,368	8,637,645	6,275,072	6,383,206	7,693,926
2	5,178,330	3,044,114	3,578,219	5,245,946	7,066,204	6,235,537	5,489,745
3	5,401,407	3,070,422	3,937,230	5,612,393	7,016,855	6,078,949	5,290,658
4	4,637,817	2,831,595	3,889,542	5,758,291	6,091,389	5,455,762	4,906,119
5	3,891,214	3,247,526	3,645,096	5,103,965	5,744,879	4,988,120	4,538,325
6	3,267,324	3,164,236	4,020,216	5,460,153	5,474,785	4,848,714	4,177,280
7	2,659,606	2,389,337	3,750,640	4,790,717	5,532,541	4,318,627	4,096,707
8	2,589,179	2,858,749	3,336,490	4,195,596	5,310,154	3,561,141	3,997,252
9	2,371,284	2,815,115	3,266,982	3,793,813	4,959,532	3,411,824	3,621,125
10	1,970,900	2,369,583	3,634,334	3,501,992	4,760,762	3,093,288	3,019,061
11	1,993,842	1,812,933	2,916,215	3,118,066	4,111,168	2,555,359	2,688,247
12	1,922,109	2,107,465	2,350,875	2,651,209	3,395,215	2,345,094	2,154,191
13	1,728,859	2,006,236	2,152,245	2,048,498	3,053,978	1,817,792	1,853,071
14	1,604,987	1,883,500	1,779,411	1,773,982	2,655,192	2,034,745	1,579,960
15	1,756,013	1,522,106	1,517,375	1,340,324	2,297,338	2,005,306	943,031
16	1,460,064	1,186,117	1,332,724	1,484,634	2,060,268	1,724,017	905,260
17	977,212	1,499,382	1,481,112	1,461,282	1,837,363	1,694,460	995,978
18	823,823	1,548,955	1,608,184	1,224,570	1,352,473	1,635,050	813,554
19	774,496	1,269,772	1,209,137	968,735	1,176,992	1,392,895	971,408
20	698,188	1,382,187	1,319,579	1,127,864	1,185,787	1,083,830	692,469
21	780,029	1,171,781	1,333,448	920,648	1,042,197	938,551	831,398
22	924,614	937,270	1,701,557	936,272	1,066,792	1,005,588	910,212
23	944,311	1,153,095	1,456,244	1,137,855	717,404	1,077,823	926,649
24	1,021,279	836,375	1,493,841	1,130,820	642,466	832,628	812,834
25	1,114,549	703,968	1,222,938	962,846	398,707	505,077	815,281

SC_{av} = average sand circle diameter (mm)

Table A2 Image group ring FFT values, sand circle measurements, and calculated average texture depth.

Image Group	A	D	E	G	H	I	J
Sand circle (mm)	191	173	142.5	179	161.25	289	265
Ring 1-20 average FFT	2,713,938	2,553,320	2,967,999	3,464,984	4,067,987	3,333,186	3,021,368
Average texture depth (mm)	1.57	1.91	2.82	1.79	2.20	0.69	0.82
Ring 1-25 average FFT	2,362,542	2,234,756	2,662.720	2,975,525	3,409,021	2,840,935	2,558,950

Road surface texture measurement using digital image processing and information theory

Land Transport New Zealand
Research Report 290